PHYSICAL REVIEW B VOLUME 36, NUMBER 13 1 NOVEMBER 1987

Static and dynamic magnetic properties of ^{3}He confined by fluorocarbon microspheres

A. Schuhl, S. Maegawa,* M. W. Meisel,† and M. Chapellier
Laboratoire de Physique des Solides, Université de Paris–Sud, Bâtiment 510, 91 405 Orsay, France
(Received 14 April 1987)

The magnetic properties of liquid ^{3}He confined by fluorocarbon microspheres have been studied by NMR in a large range of magnetic fields (0.03–3 T) and between 10 and 800 mK. The dynamics of the liquid magnetization are driven by the relaxation mechanisms of the adsorbed solid ^{3}He film. This relaxation is produced by the ^{3}He motion induced by quantum exchange. The spectral density of this motion has been deduced from measurements of relaxation times in the liquid. The quantum exchange in the solid layer also allows a magnetization transfer between the ^{3}He and substrate ^{19}F spins. Magnetic susceptibility measurements have also been done as function of pressure and temperature. A growth of adsorbed solid is observed as the liquid pressure increases. We also demonstrated the possibility of producing enhanced liquid ^{3}He magnetization by nuclear dynamic polarization.

I. INTRODUCTION

Interest in the surface magnetic properties of normal fluid ^{3}He dates back more than 20 years.[1] Experimentally, the magnetic surface phenomena are usually studied by using high–surface-area substrates to confine the liquid ^{3}He. Numerous experiments have been developed to study a variety of substrates containing a spectrum of characteristic sizes which provide the required surface-to-volume ratio. The surface-to-volume ratio is dictated by the experimental sensitivity of extracting the surface contribution to the ^{3}He magnetization from the background arising from the bulk liquid. In practice, the average pore diameters of materials which have been used in these studies range between 10^2 and 10^4 Å.

The van der Waals binding potential exerted by the substrate on the liquid atoms has the effect of localizing the ^{3}He situated in the neighborhood of the surface. It is well established that the substrate is separated from the liquid by at least one atomic layer of adsorbed solid. This fact has been demonstrated on grafoil by specific-heat measurements[2] and neutron-diffraction studies.[3] In addition, a universal feature of all the substrates studied is the existence of a Curie-Weiss-type contribution to the ^{3}He magnetization where at least part of this effect is generated by the surface-adsorbed atoms. There remains, however, an uncertainty in the size of the adsorbed solid thickness which seems to be substrate dependent, varying from one to a few atomic layers.

The study of confined ^{3}He systems by NMR may be grouped into two categories. Firstly, static magnetization measurements of the ^{3}He as a function of temperature furnish information about the localized and bulk liquid atoms. Secondly, dynamic investigations of the relaxation times, T_1 and T_2, permit the study of the magnetic interactions between the bulk liquid and the adsorbed solid or solidlike ^{3}He and between the ^{3}He and the substrate.

In 1976, Ahonen *et al.*[4] measured the magnetization of ^{3}He, $M_{\mathrm{He}}(T)$, confined between Mylar sheets. These workers were the first to identify the two typical contributions to $M_{\mathrm{He}}(T)$. One contribution was temperature independent and was attributed to the bulk liquid, while the second part was well described by a Curie-Weiss law, $M''_{\mathrm{He}}(T)=C/(T-\Theta)$, with $\Theta=0.5$ mK. The relative weight of the Curie-Weiss contribution varied weakly with magnetic field and was ascribed to 5 times the estimated quantity of ^{3}He contained in the first adsorbed layer. It is difficult to attribute this contribution to five or more layers of solid arising from the influence of the van der Waals potential since this potential is negligible at such large distances. Following this work, Spanjaard *et al.*[5] proposed that the Curie-Weiss contribution could arise from the liquid in the second or third atomic layers. In this ferromagnetic liquid model, the van der Waals potential V_B that the boundary exerts on the liquid causes an increase in the density of states at the Fermi surface. Consequently, the liquid susceptibility is increased, and the liquid closest to the substrate may be ferromagnetic if the potential V_B is sufficiently large. This description seemed to be confirmed by results that were obtained by Ahonen *et al.*[6] using Carbolac as a confining substrate. At about the same time, experiments conducted in Grenoble by Godfrin *et al.*,[7] using continuous-wave NMR to study various substrates (alumina powder, Grafoil, platinum powder), indicated that the relative weight of the Curie-Weiss-type contribution corresponded to, within 10%, only the ^{3}He contained in the first adsorbed layer. Bozler *et al.*[8] have observed, by pulsed NMR studies of ^{3}He confined by Grafoil, the same behavior that was observed in Grenoble. Finally, experiments[9] performed with the assistance of SQUID (superconducting quantum-interference device) techniques on silver powder have established the existence of a ^{3}He magnetization contribution of Curie-Weiss type which is equivalent to five atomic layers. In view of the large differences in the numbers of "solidlike" or Curie-Weiss layers, it appears to us important to

calibrate, in a direct manner, the number of atoms with a Curie-Weiss behavior. This was possible here because we could produce a monolayer, calibrate this monolayer against the number of fluorine atoms, and later compare the number of atoms following a Curie-Weiss law to the number of atoms in the monolayer. Bulk solid ^{3}He at low pressures has a bcc structure and possesses an antiferromagnetic nature.[10] On the other hand, bulk solid ^{3}He at high pressures has a hcp structure and exhibits ferromagnetic tendencies with a Weiss temperature $\Theta \sim 30$ μK.[11] At the same time, the magnetization of bulk liquid ^{3}He is limited by Fermi statistics and, hence, assumes an approximately temperature-independent constant value below its magnetic Fermi temperature.[12] Therefore, the surface magnetism of ^{3}He is indeed an interesting phenomenon since it obeys a Curie-Weiss law with ferromagnetic Θ values which are almost substrate independent and range between approximately 0.3 and 0.8 mK. Secondly, the presence of ^{4}He completely destroys this behavior and causes the magnetization to be given by bulk liquid ^{3}He. This ^{4}He effect is well documented[13] and is a consequence of the ^{4}He displacing the surface ^{3}He due to the higher zero-point energy of the ^{3}He. In this paper we will not dwell on the role that ^{4}He plays on our substrate as appropriate reports have appeared elsewhere.[14,15]

Using the fluorocarbon microspheres of Dupont DLX-6000, measurements performed at Orsay[15–17] (see Sec. IV A) and Cornell[18] have shown that the Curie-Weiss contribution to the ^{3}He magnetization corresponds to 1.45 times the number of spins contained in the first adsorbed layer, N_0. This result may be attributed either to an ensemble of $1.45N_0$ localized spins or one adsorbed solid layer and one liquid layer close to a ferromagnetic instability. In an attempt to answer the question of the nature of the layer responsible for the Curie-Weiss contribution, we have studied the ^{3}He magnetization as a function of the liquid pressure. To first order, the adsorbed solid properties are expected to be relatively independent of external pressures less than 34 bars since the effective internal pressure of this layer is on the order of approximately 400 bars, Ref. 19. On the other hand, the bulk liquid magnetization per atom is strongly pressure dependent due, in part, to changes in the density of states at the Fermi level.[12] Although the idea has not been discussed theoretically,[5,20] one might reasonably hypothesize[15] that a two-dimensional Fermi liquid near a ferromagnetic instability could be dramatically affected by pressure changes in a manner similar to the bulk liquid. Our experimental results which address this question will be presented and discussed in Sec. IV.

With respect to the T_1 of the liquid, the first confined-geometry measurements which indicated the importance of the surface on the relaxation mechanisms were reported by Kelly and Richardson,[21] who studied ^{3}He confined by Carbolac powder. The observed relaxations were shorter than those of bulk ^{3}He, Ref. 22, by a factor of 10^3 over a temperature range 0.05–0.3 K. These authors also established that the variation of the ^{3}He spin-lattice relaxation time with temperature, $T_1^{\mathrm{He}}(T)$, was unusual, in that below 0.3 K the function $T_1^{\mathrm{He}}(T)$ decreased with temperature. Additional evidence from a variety of other substrates[7,16,23] indicates that T_1^{He} is proportional to T below 100 mK. Hammel and Richardson[24] (HR) have proposed a model to explain this universal, substrate-independent temperature dependence of T_1^{He}. Several important ingredients to the HR work were initially identified by Sullivan.[71] In the HR model, all of the bulk liquid is assumed to relax through the magnetization of the solidlike adsorbed layer whose internal relaxation processes are taken to be independent of temperature. Furthermore, other experiments conducted with different substrates[21,23,25,26] have shown that T_1^{He} varies linearly with applied magnetic field, or equivalently, with the ^{3}He nuclear Larmor frequency, ν_{He}. Cowan[27] has proposed an explanation of this dependence in which the relaxation of the adsorbed layer will be due to a modulation of the ^{3}He-^{3}He dipolar interaction by the movements introduced by exchange. The spectral density of these movements in a plane will give a linear dependence of T_1^{He} with ν_{He} over a small range of frequency in the neighborhood of the exchange frequency ν_{He}. The work that will be presented in Sec. V was performed with the objective of, firstly, testing the generality of the HR model and, secondly, observing the dependence of T_1^{He} on ν_{He} over a large frequency range. We have therefore measured T_1^{He} for temperatures between 10 and 800 mK and for frequencies varying between 125 kHz and 100 MHz. We have also extended these measurements to the ^{3}He spin-spin relaxation time, T_2^{He}, at the lower frequencies. A brief report of the initial part of this work has already appeared.[17]

All of the experiments conducted down to the lowest temperatures of approximately 1 mK suggest the ^{3}He magnetization exhibits ferromagnetic behavior with Θ values between 0.3 and 0.8 mK.[4,6–9,18,23,28] It is rather remarkable that the Θ values show little substrate dependence while the size of the Curie-Weiss contribution, normalized to the number of atoms in the first atomic layer, varies between one and five layers from one substrate to another. Various hypotheses have been formulated to explain these ferromagnetic deviations: an exchange between the spins of the liquid and those of the solid,[29,30] the presence of a ferromagnetic liquid layer,[5,31] the presence of vacancies in the solid layer,[32–34] or an internal exchange of solid particles in the event that more than one layer solidifies.[35] Unfortunately, our experimental apparatus would not permit us to attain the temperature range where these deviations could be observable. However, the study of the spin dynamics at high temperature, in addition to our knowledge of the nature of the Curie-Weiss contribution, enables us to draw several conclusions about the magnetic properties of ^{3}He confined by fluorocarbon microspheres. Section VI will be devoted to this discussion.

To begin our discussion, Sec. II, we will first describe the fluorocarbon substrate, and we will find it useful to describe the ^{3}He-^{19}F magnetic coupling. Section III will be devoted to detailing the pertinent experimental conditions. Then as mentioned above, Sec. IV will describe our static measurements, Sec. V will contain a presentation of our dynamic studies, and Sec. VI will discuss the

nature of the exchange in the adsorbed solidlike layer. In Sec. VII we shall close by summarizing our work and interpretations and by suggesting possible future directions.

II. THE SUBSTRATE AND THE ADSORBED ^{3}He-^{19}F MAGNETIC COUPLING

The substrate that we have studied consists of microspheres of a fluorocarbon polymer sold under the trade name DLX-6000 by Dupont.[36] Scanning-electron micrographs performed by Friedman *et al.*[37] show that the spheres have a uniform diameter of approximately 2×10^3 Å. The isotherms performed on this substrate at 77 K with nitrogen[37,38] suggest that a monolayer of ^{3}He corresponds to 3.8 cm^3 STP per gram of DLX-6000.

A. Evidence of magnetic coupling

In studying the magnetic properties of an atomic monolayer of ^{3}He adsorbed on fluorocarbon microspheres, Friedman *et al.*[39] discovered the existence of a strong magnetic interaction between the ^{19}F nuclei localized in the substrate and the ^{3}He spins situated at the surface. This coupling is *a priori* surprising since one would expect the surface to be exempt of magnetic impurities due to the inert character of the fluorocarbon. In general, the magnetic interactions between the ^{3}He liquid and the adjacent solid are not well understood. It seems that the magnetic interactions are responsible, in certain cases,[1] for a thermal surface conduction between the solid and the ^{3}He which at low temperatures becomes larger than those due to acoustic processes.[40] We shall restrict our discussion to normal fluid ^{3}He and will not comment on either the thermal, magnetic, acoustic, or quasiparticle behavior of superfluid ^{3}He in contact with a boundary.[18,23,41] The interest in DLX-6000, with respect to the other systems used to study these interactions, resides in the possibility of simultaneously measuring the respective magnetizations of the ^{19}F and the ^{3}He, i.e., M_F and M_{He}. This permits, in particular, the perturbation of one of the two magnetizations in order to study the induced variations of the other. This possibility is illustrated in Fig. 1, which shows the results of Friedman *et al.*[37,39] on an atomic monolayer of ^{3}He adsorbed on DLX-6000 in 1.1 kG at 1.0 K. Figure 1(a) shows the return to equilibrium of M_F after it has been tipped by a π pulse at the ^{19}F Larmor frequency at 1.1 kG, $\nu_F=4.45$ MHz. This pulse should not affect M_{He} because the resonance frequency of the ^{3}He, $\nu_{He}=3.56$ MHz, is sufficiently far from ν_F that the two linewidths do not overlap. However, M_{He} tips instantly, Fig. 1(b), and returns to its equilibrium value M^0_{He} with a characteristic time identical to that of the ^{19}F, $T_1^F=40$ sec [Fig. 1(a)]. On the other hand, for a π pulse at the ^{3}He frequency, M_{He} is tipped, M_F is not affected, and M_{He} relaxes, Fig. 1(c), with a characteristic time $T_1^{He}\simeq40$ msec, substantially shorter than T_1^F. The asymmetry between these two experiments is due to the fact that M_F is much larger than M_{He}. Previous Orsay measurements,[16] performed under slightly different conditions, yielded $M_F/M_{He}\simeq316$. It is important to note that all the ^{19}F magnetization must be considered because the diameter of the spheres is small enough to ensure the diffusion of the interior magnetization is faster than the ^{19}F relaxation. Friedman *et al.*[37,39] have shown that the intrinsic relaxation of M_F is negligible. In fact, after replacing the ^{3}He by ^{4}He, T_1^F is increased by a factor of 10 at 1 K and 30 at 0.4 K in a field of 0.1 T.

One possible relaxation diagram that the above experiment suggests is presented in Fig. 2. The ^{19}F magnetization relaxes through the Zeeman-energy bath of the ^{3}He adsorbed layer. The magnetization transfer between the

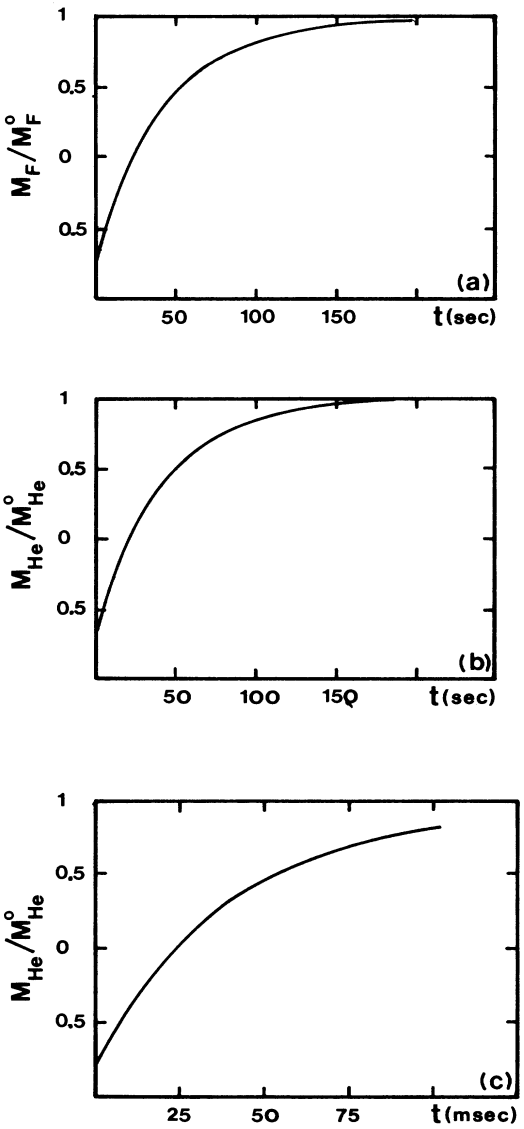

FIG. 1. First observation of the magnetic interaction between ^{3}He and ^{19}F. This experiment was performed at Cornell in a field $B=1.1$ kG at $T=1$ K (Refs. 37 and 39). (a) After a π pulse on the fluorine spins, the ^{19}F magnetization relaxes within a time $T_1^F=40$ sec, and (b) the ^{3}He magnetization, M_{He}, follows exactly the fluorine magnetization. (c) After a π pulse on the ^{3}He spins, M_F is not perturbed and M_{He} relaxes within a time $T_1^{He}\simeq40$ msec.

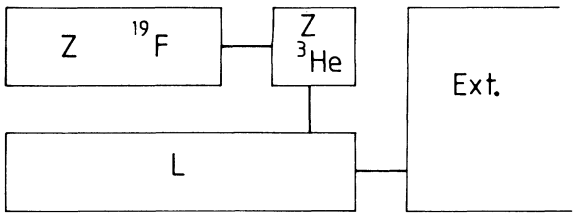

FIG. 2. The simplest relaxation-pathway mode: the ^{19}F Zeeman bath relaxes to the lattice through the ^{3}He Zeeman bath. The lattice is in strong thermal contact with the mixing chamber (labeled ext.) which may be considered a thermostat.

two Zeeman baths is, however, mysterious due to the energy difference between $h\nu_F$ and $h\nu_{He}$. The purpose of our experiments was to understand this magnetic interaction. Magnetic impurities, particularly adsorbed oxygen, would, in general, be good candidates for explaining any peculiar magnetic phenomena at the surface. The role and properties of magnetic impurities will be studied in the following subsection, before showing, with the assistance of our experiments, that the origin of the coupling is due to the internal properties of the ^{3}He surface layer.

B. Magnetic impurities

1. Oxygen

DLX-6000 is an attractive substrate because of the weak chemical reactivity of the C—F bond. Although this property diminishes the possibility of the surface attracting various magnetic impurities, oxygen always remains a possible candidate. The experiments performed at Cornell have usually been executed only after the microspheres were "cleaned" in the following manner. Firstly, after the cell was mounted, the sample was heated to near 100 °C. Next, the experimental cell was pumped at this temperature for about 1 week. Periodically, the pumping was interrupted to introduce nitrogen gas into the cell, and the pumping was resumed. Following these precautions, it was hoped that the magnetic impurities initially present on the surface could be eliminated. This procedure was originally introduced by Friedman *et al.*[37,38] Furthermore, these authors also performed experiments with a "dirty" sample surface, i.e., one that has not been cleaned. The ^{3}He relaxation was observed to be independent of the quality of the surface, but the ^{19}F relaxation time was decreased by a factor of 10–100 from the "cleaned"-surface value. The oxygen, therefore, has no effect on the coupling, but accelerates the intrinsic relaxation of the ^{19}F. The explanation of this result will be given later as we remark here that the important oxygen atoms are not those adsorbed on the surface, as was thought initially, but are those trapped in the volume of the substrate.[42]

It is well known that the DLX-6000–type polymer may contain a high concentration of electronic centers if it has been strongly irradiated by γ rays.[43–46] These electronic impurities are situated at the defects of the C-F chain where a ^{19}F atom has been ejected, Fig. 3(a). The γ-ray irradiation of DLX-6000 during fabrication was not known since this process is apparently protected as an industrial secret. However, an electronic resonance study made by Chapellier *et al.*[42] has proven the existence of 2.6×10^{18} electronic centers per cm^3 of DLX-6000. In addition, these authors have shown that the form of the electronic linewidth, the variation of the linewidth form with temperature, and the changes observed on the linewidth when the powder is pumped at 100 °C are identical to those results obtained from highly irradiated fluorocarbon.[43,46] Therefore, it seems that DLX-6000 was indeed irradiated during fabrication. In the presence of oxygen, the electronic centers transform into peroxide centers, Fig. 3(b). The properties of these centers have been extensively studied in fluorocarbon, i.e., polytetrafluorethylene.[45,46] In particular, these studies have shown that (i) the g factor of these centers is anisotropic, $g_{\parallel}=2.002$ and $g_{\perp}=2.038$; (ii) the Cornell cleaning formula is a reversible process; and (iii) it is possible to irreversibly eliminate the electronic centers by annealing at temperatures close to the disassociation temperature of the polymer, $T_d\sim310$ °C. This final point has been verified for DLX-6000, Fig. 4, Ref. 16.

2. Electrons

Chapellier[47] has proposed that the ^{3}He-^{19}F magnetic coupling could be attributed to the existence of paramagnetic electronic moments. In this type of explanation, each of the Zeeman nuclear baths would be strongly coupled to the energy bath of spin-spin electronic interactions. Such a mechanism has been observed in lithium fluoride.[48] The subsequent discovery of a large concentration of electronic centers in DLX-6000, Ref. 42, enhanced the attractiveness of Chapellier's proposition. The elementary mechanisms of coupling between the electrons and the nuclei may be understood in simple terms. To start, the broadening of the electronic Larmor frequency must be large compared to the nuclear resonance frequency. Then, an electronic spin flip-flop could invert a nuclear spin.[49] However, when the electronic polarization P increases, the number of

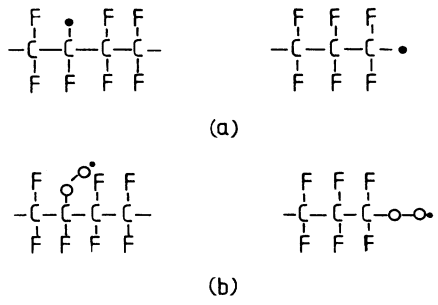

FIG. 3. (a) When the fluorocarbon is γ-irradiated, sites where ^{19}F spins are ejected form electronic centers. (b) As oxygen is introduced, the O_2 molecules are trapped, forming peroxide centers.

electronic flip-flops decreases, causing the electron-nuclei relaxation rate to diminish as $1-P^2$. Experimentally, the ^{3}He-^{19}F coupling remains efficient even under conditions of high magnetic field and low temperature, where the electronic spins are totally aligned, i.e., $P=1$ (Refs. 16 and 23). Moreover, the annealing process may eliminate about 99% of the electronic centers, Fig. 4, but this heat treatment has no effect on the strength of the ^{3}He-^{19}F magnetic coupling.[16] These observations lead us to conclude that the electronic centers are not involved in the ^{3}He-^{19}F magnetic interaction. However, we have exploited, following Chapellier's ideas,[47] the electronic centers to conduct dynamic nuclear polarization studies; see Sec. V D.

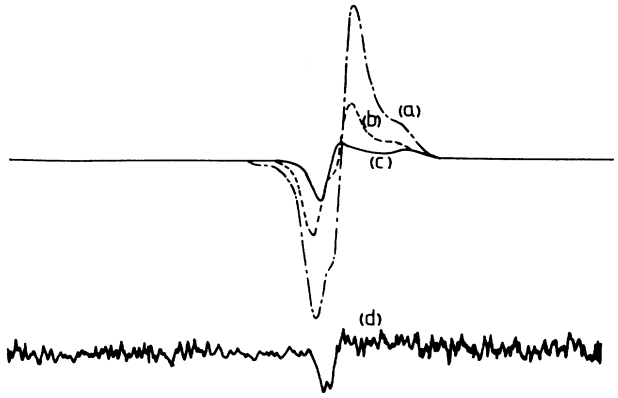

FIG. 4. EPR signal of the fluorocarbon beads (a) without any treatment, and after 3 h at (b) 200 °C, (c) 250 °C, and (d) 295 °C. The gain for signal (d) is 40 times larger than for the three other signals (Ref. 16).

C. Coupling models

From the preceding discussion, we have seen that the relaxation model presented in Fig. 2 cannot explain the magnetization transfer between the two spin systems. In order to satisfy conservation of energy, it is necessary to introduce a third energy bath in the coupling mechanism. This additional bath may act in two distinct ways. The first possibility, indirect coupling, may also be called an "energy transformer." It is a bath strongly coupled with each of the two Zeeman energy baths, and hence, the internal transitions permit the adsorption and emission of the two quanta, $h\nu_F$ and $h\nu_{He}$. In the relaxation process proposed by Chapellier,[47] the electronic dipolar energy plays this type of role. In order to explain the experimental results, the transformer must have a small specific heat with respect to those of the Zeeman baths and an internal relaxation time short compared to the other characteristic times of the system, particularly T_1^{He}. Alternatively, a direct coupling mechanism may function between the ^{19}F and the ^{3}He. A third energy bath must be present and capable of furnishing or receiving the energy difference $h(\nu_F-\nu_{He})$. The movements of the ^{19}F and ^{3}He atoms modulate the dipolar interaction between the two spin species. These motions would be capable of introducing an energy transfer between the two Zeeman baths if the spectral density of the movement was large enough at $\nu=(\nu_F-\nu_{He})$. We can immediately reject the possibility of a role played by the ^{19}F motion since the temperature is too low. Moreover, if they were responsible for the high-frequency coupling [$(\nu_F-\nu_{He})\sim 10$ MHz], they would relax the ^{19}F directly at low frequencies ($\nu_F<10$ MHz), which would be in contradiction with the measurements of Freidman *et al.*,[37,39] Sec. II A. In the adsorbed layer, the atomic motion introduced by quantum exchange is a good candidate for the direct-coupling-type mechanism. We develop these two models in the following two subsections and compare them with experimental results of Schuhl *et al.*,[16] Table I.

1. Indirect coupling

The first of the two possible coupling modes involves an intermediate-energy bath which, as we have already discussed, is not related to the electronic centers. We shall show briefly that this mechanism is not compatible with the experimental results.[16]

The relaxation diagram corresponding to an indirect mechanism is presented in Fig. 5. The form of the equations of motion of the system do not depend on the nature of the intermediate bath as long as its specific heat is small and its internal equilibrium times are short. In the high-temperature limit ($h\nu \ll k_B T$) we are able to define a spin temperature T_S for the magnetization value $M=C/T_S$. Defining $\beta=1/k_B T_S$, the evolution of the system is given by[49]

TABLE I. Experimental values of ^{19}F and ^{3}He relaxation times when one atomic layer of ^{3}He is adsorbed at the surface of the DLX-6000 microspheres. The ratio R is defined by Eq. (4).

B (T)	ν_{He} (MHz)	ν_F (MHz)	T (mK)	T_1^{He} (sec)	T_1^F (min)	R (%)
0.77	25	30.8	550	0.5	9.3	13.5
1.54	50	61.8	200	1.8	34	16.5
			350	1.6	28	21.5
			600	1.5	26	21
3.08	100	123.5	350	3.7	71	9

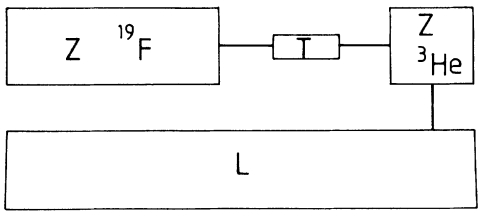

FIG. 5. Coupling model with an intermediate bath of electronic centers. In this model all the energy of the ^{19}F relaxes to the lattice through the ^3He Zeeman bath.

$$\frac{d\beta_F}{dt}=x^2\frac{1}{T_c}(\beta_{He}-\beta_F)\ ,$$
$$\frac{d\beta_{He}}{dt}=\frac{1}{T_c}(\beta_F-\beta_{He})+\frac{1}{T_1}(\beta^0_{He}-\beta_{He})\ , \tag{1}$$

with

$$x^2=\frac{N_{He}}{N_F}\frac{\gamma^2_{He}}{\gamma^2_F}\ , \tag{2}$$

where N_{He} and N_F are the number of spins of the two species and γ_{He} and γ_F are their gyromagnetic ratios. In Eq. (1), $1/T_c$ is the relaxation rate between the ^3He and the ^{19}F, while $1/T_1$ is the Zeeman-lattice relaxation rate for the ^3He. These equations yield two time constants for the system that, in our case ($x^2\ll 1$), may be attributed to T_1^{He} and T_1^F. The three measurables are given by

$$T_1^{He}=\left[\frac{1}{T_1}+\frac{1}{T_c}\right]^{-1}\ ,$$
$$T_1^F=\frac{1}{x^2}(T_1+T_c)\ , \tag{3}$$

and

$$R=\frac{T_c}{T_1+T_c}\ .$$

From the experimental values of T_1^{He}, T_1^F, and R, we may deduce the parameters T_1, T_c, and x^2, for each magnetic field B and each temperature T, Table II. Experimentally, the ratio R is defined by

TABLE II. Parameters of the model of indirect coupling deduced from experimental data (Table I). The parameter x^2 should be constant [Eq. (2)].

B (T)	T (mK)	T_c (sec)	T_1 (sec)	$1/x^2$
0.77	550	0.58	3.7	130
1.54	200	2.1	11.3	125
	550	2.0	7.6	183
	600	1.9	7.3	172
3.08	350	4.1	41.1	95

$$R=\frac{M_{He}(M_F=0)}{M_{He}(M_F=M_F^0)}=\frac{M_{He}(M_F=0)}{M_{He}^0}\ , \tag{4}$$

where $M_{He}(M_F=0)$ is the M_{He} value after M_F has been saturated by an oscillating field and M_i^0 represents an equilibrium value.

The value of x^2 predicted by this model varies enormously from one (B,T) point to another, where, by definition, this parameter must remain constant. The average value of x^{-2} is about 2 times weaker than the value, $x^{-2}=316$, determined directly from the measurement of N_F/N_{He}. We are led to conclude that experimental results[16] exclude this model of indirect coupling between the ^3He and the ^{19}F.

2. Direct coupling

In this subsection we consider the magnetization transfer between the two Zeeman baths due to the modulation of the ^3He-^{19}F dipolar interaction by the motion in the adsorbed layer. In the three-dimensional solid, the ^3He-^3He dipolar interaction is modulated by the exchange movements which are responsible for the Zeeman-lattice relaxation for temperatures below 1 K (Refs. 50 and 51). We shall begin by briefly reviewing the method of calculating the relaxation times T_1 and T_2 in solid ^3He.

The Hamiltonian H of the solid ^3He system may be written as the sum of three terms,

$$H=H_Z+H_e+H_d\ , \tag{5}$$

where H_Z is the Zeeman energy, H_e is the exchange Hamiltonian, and H_d is the dipolar interaction. Since $[H_Z,H_e]=0$, a direct energy exchange does not exist between the two baths of Zeeman and exchange energy. These baths are indirectly coupled by H_d, which does not commute with either of the two Hamiltonians H_Z or H_e. The dipolar interaction may be decomposed in the following manner:[52]

$$H_d=\sum_{m=-2}^{+2}D_m\ ,$$
$$D_m=\hbar^2\gamma^2\left[\frac{4\pi}{5}\right]^{1/2}\sum_{i<j}[Y_2^{-m}(\Omega_{ij})T_{ij}^m(-1)^m]/r_{ij}^3\ , \tag{6}$$

where Ω_{ij} represents the direction of vector $\mathbf{r}_{i,j}$, Y_z^m is the second-order spherical harmonic, and the tensors T_{ij}^m are the second-order invariants:

$$T_{ij}^0=\mathbf{I}^i\mathbf{I}^j-3I_z^iI_z^j\ ,$$
$$T_{ij}^1=\sqrt{3/2}(I_z^iI_+^j+I_z^jI_+^i)=-(T_{ij}^{-1})^*\ , \tag{7}$$
$$T_{ij}^2=-\sqrt{3/2}I_+^iI_+^j=(T_{ij}^{-2})^*\ .$$

The dipolar interaction provides a weak perturbation on the system. The relaxation times, calculated by developing the logarithm of the relaxation functions in powers of H_d (Refs. 53 and 54), are then given by the following relations:

$$\frac{1}{T_1}=J_1(\omega_0)+J_2(2\omega_0)\ ,$$
$$\frac{1}{T_2}=\tfrac{3}{2}J_0(0)+\tfrac{5}{2}J_1(\omega_0)+J_2(2\omega_0)\ . \tag{8}$$

In these expressions, the spectral densities $J_m(\omega)$ are the Fourier transforms of the correlation functions $G_m(\tau)$ defined by

$$G_m(\tau)=\mathrm{Tr}[D_m(0)D_{-m}(\tau)]/\mathrm{Tr}I_z^2\ . \tag{9}$$

The generalization of the above approach to the two-dimensional case has been the subject of numerous studies.[55] In particular, Cowan[56] has obtained an expression for the spectral densities for an exchange Hamiltonian of the Heisenberg nearest-neighbor type. The decrease of the correlation functions $G(t)$ for times greater than the inverse of the exchange frequency varies as $1/t$ and is characteristic of diffusion in an infinite plane.[57] Moreover, the spectral densities $J_0(\omega)$, $J_1(\omega)$, and $J_2(\omega)$ are not necessarily equal and, in addition, may depend on the direction of the field with respect to the plane. In order to apply the above results to the interaction between ^{3}He and ^{19}F, we shall follow an approach based on the elaborate treatment given for the HF molecule.[15,18,58] The equations of motion for M_F and M_{He} are then, in the high-temperature limit $h\nu \ll k_BT$,

$$\frac{1}{\gamma_{He}}\frac{dM_{He}}{dt}=-\rho_{He}\frac{1}{\gamma_{He}}(M_{He}-M_{He}^0)+\sigma\frac{1}{\gamma_F N_F}(M_F-M_F^0)\ ,$$
$$\frac{1}{\gamma_F}\frac{dM_F}{dt}=\sigma\frac{1}{\gamma_{He}}(M_{He}-M_{He}^0)-\rho_F\frac{1}{\gamma_F}-(M_F-M_F^0)\ , \tag{10}$$

with

$$\rho_H=\delta_{HF}[\tfrac{1}{12}J_0(\omega_F-\omega_H)+\tfrac{3}{2}J_1(\omega_H)+\tfrac{3}{4}J_2(\omega_F+\omega_H)]\ ,$$
$$\rho_F=\delta_{HF}[\tfrac{1}{12}J_0(\omega_F-\omega_H)+\tfrac{3}{2}J_1(\omega_F)+\tfrac{3}{4}J_2(\omega_F+\omega_H)]\ ,$$
$$\sigma=\delta_{HF}[\tfrac{1}{12}J_0(\omega_F-\omega_H)-\tfrac{3}{4}J_2(\omega_F+\omega_H)]\ ,$$

and

$$\delta_{HF}=\langle 1/r^6\rangle\gamma_{He}^2\gamma_F^2\hbar^2\ .$$

In these expressions, r designates the distance between the two ^{19}F and ^{3}He nuclei and $\langle 1/r^6\rangle$ is a time-averaged value. The experiments[16] were performed at frequencies large compared to the average exchange frequency, so these expressions may be simplified by keeping only the $J_0(\nu_{He}-\nu_F)$ terms and neglecting those of higher order. The terms $J_1(\nu_{He})$ and $J_1(\nu_F)$ represent a direct relaxation of each Zeeman bath toward the ^{3}He exchange bath, while the terms $J_0(\nu_F-\nu_{He})$ introduce a magnetization transfer between these two spin baths.

In order to write the magnetization relaxations for M_F and M_{He}, it is necessary to take into account not only the ^{3}He-^{19}F interaction given by Eq. (10), but also the intrinsic relaxation of M_{He} towards the lattice, i.e., we must add a term,

$$-\frac{1}{T_1\gamma_{He}N_{He}}(M_{He}-M_{He}^0)\ , \tag{11}$$

to the first expression in Eq. (10). Before continuing, several precautions must be recalled because the relaxation in the two-dimensional ^{3}He layer is also ascribable to the modulation of the ^{3}He-^{3}He dipolar interaction by the motion of the ^{3}He atoms experiencing exchange. These are *a priori* the same movements, and therefore the same spectral densities would enter into the two mechanisms. It may appear less rigorous to neglect the terms $J_1(\nu_{He})$ and $J_1(\nu_F)$ in Eq. (10), while the same terms appear in the ^{3}He Zeeman-lattice relaxation, Eq. (11). We are, however, able to reasonably make this approximation for the following reasons. Firstly, the number of ^{3}He nearest neighbors for a ^{19}F atom is on the order of one or two and not six as for a ^{3}He atom. Secondly, we speculate that the most mobile ^{3}He atoms are those which are less bound to the surface and are also the furthest from the ^{19}F. Finally, the theoretical analysis and the experimental results[16] are in good agreement despite this approximation. In the end we will discuss the effect of terms which have been presumed to be negligible. The equations of motion for the system composed of N_{He} spins of ^{3}He and N_F spins of ^{19}F may now be rewritten from Eq. (10) in the form

$$\frac{dm_F}{dt}=\frac{N_{He}}{N_F}\frac{1}{T_c}[(m_{He}-m_{He}^0)-(m_F-m_F^0)]\ ,$$
$$\frac{dm_{He}}{dt}=\frac{1}{T_c}[(m_F-m_F^0)-(m_{He}-m_{He}^0)]-\frac{1}{T_1}(m_{He}-m_{He}^0)\ , \tag{12}$$

where m represents the polarization defined for each species taken from the spin states $\uparrow$ and $\downarrow$ by the relation

$$m=[n(\uparrow)-n(\downarrow)]/[n(\uparrow)+n(\downarrow)]\ .$$

The second term of the second expression in Eq. (12) is the intrinsic relaxation of ^{3}He toward the exchange bath, assuming this bath is in good thermal contact with the lattice. The times T_1 and T_c are expressed as a function of the spectral density $J_0(\nu)$ and are considered as model parameters. The resolution of Eq. (12) yields the following expressions for T_1^{He}, T_1^F, and R, namely

$$T_1^{He}=\left[\frac{1}{T_1}+\frac{1}{T_c}\right]^{-1}\ ,$$
$$T_1^F=\left[\frac{N_F}{N_{He}}\right](T_1+T_c)\ , \tag{13}$$

and

$$R=1-\left[\frac{\gamma_F}{\gamma_{He}}\right]\frac{T_1}{T_1+T_c}\ .$$

Thus, starting from the experimental values[16] of T_1^{He}, T_1^F, and R (Table I), the direct-coupling model yields the parameters T_1 and T_c, and one value of N_F/N_{He} which is compatible with Eq. (13), see Table III. The model es-

TABLE III. Parameters of the direct-coupling model, where T_1 is the Zeeman-lattice relaxation time of ^{3}He and T_c is the coupling time.

B (T)	T (mK)	T_c (sec)	T_1 (sec)	N_F/N_{He}
0.77	550	0.71	1.7	232
154	200	2.6	5.8	243
	350	2.5	4.5	240
	600	2.4	4.2	236
3.08	350	5.0	14.1	223

timate of $N_F/N_{He}=235$ ($\pm 10\%$) is in good agreement with the directly determined value of $N_F/N_{He}=207$ ($\pm 10\%$).

Figure 6 shows the relaxation diagram for the direct-coupling model. For the ^{19}F relaxation, part of the energy leaves directly through the exchange bath of ^{3}He, which is represented by the dotted line. The approximations that have been made consist of neglecting a direct relaxation of M_F through the ^{3}He exchange bath. Taking into account this additional path, marked by the dashed line in Fig. 6, would increase the estimated ratio N_F/N_{He} and introduce a small discrepancy between the model and the experiments.[16]

In the direct-coupling model, the exchange was assumed to be in good thermal contact with the lattice. The increase of T_1^F observed[16] for $T<200$ mK, Fig. 7, may be a simple illustration of the decoupling of the exchange bath to the lattice, as is observed, in the same temperature range, for the three-dimensional solid.[51] This may also be interpreted as a decrease of the lattice specific heat to a limit where it is no longer a good thermal reservoir with respect to the ^{19}F Zeeman energy. The relaxation would then involve the coupling between the lattice and the true thermal reservoir comprised of

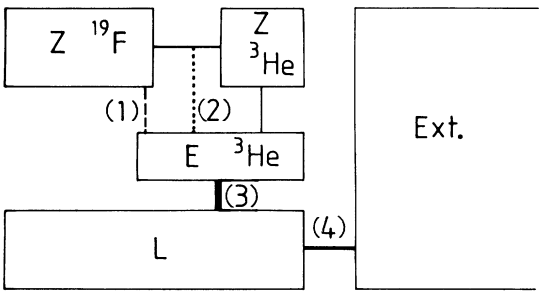

FIG. 6. Direct ^{3}He-^{19}F coupling model. The exchange in the ^{3}He solid layer produces a modulation of the nuclear dipolar interaction. In this model a part of the ^{19}F energy relaxes to the lattice directly through the ^{3}He exchange bath, which is assumed to be at the lattice temperature. Most of the ^{19}F energy relaxes through the ^{3}He Zeeman bath. This channel drives the relaxation. Several interaction paths are labeled for reference purposes and are used during the course of a discussion in the text.

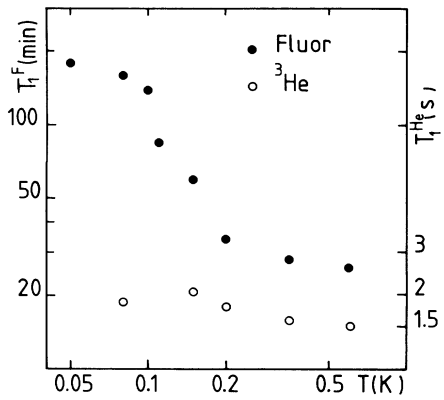

FIG. 7. Relaxation times T_1^F and T_1^{He} of the fluorine and ^{3}He magnetization when one layer of ^{3}He atoms is adsorbed on the fluorocarbon substrate in $B=1.5$ T, Ref. 16.

the mixing chamber of the dilution refrigerator. In the last case it is difficult to estimate the lattice specific heat due to the influence of the phonons on the adsorbed layer and the substrate. Both explanations are in accordance with the fact that, if liquid is added to the system, T_1^F does not show any increase down to at least 10 mK. A detailed study of the relaxation of ^{19}F in the presence of a ^{3}He monolayer,[59] particularly its deviations from exponential, would permit the identification of the cause of the T_1^F increase. Such an experiment requires an improvement on the precision of the M_F measurements and, in addition, the elimination of all parasitic heating since the observed relaxation time is comparable to the global thermal equilibrium times of the experimental cell.

Finally, we note that the direct-coupling model requires the existence of elevated exchange frequencies. In fact, for 3.1 T the difference in energy $[h(\nu_F-\nu_{He})]$ corresponds to a temperature of approximately 1 mK. This value is approximately 2 orders of magnitude larger than the value expected of a two-dimensional solid with a molar volume equal to that of the adsorbed layer sitting in a potential well of ~ 60 K in depth.[35,60] In addition, if all the ^{3}He spins contribute to the spectral density $J_0(\nu)$ at this frequency, the system would exhibit interesting properties at temperatures near 1 mK. In particular, the susceptibility χ of the ^{3}He would show deviations from a Curie-Weiss law in this range of temperature, and at even higher temperatures since the ^{3}He-^{19}F coupling has been observed for larger magnetic fields,[61] even as high as 12 T (Ref. 62). Our understanding and explanation of these properties will be described in Secs. IV, V, and VI, with the latter section containing the most detailed discussion.

III. EXPERIMENTAL CONDITIONS

With the exception of some dynamic nuclear polarization work to be described in Sec. V D, all of our work involves nominally pure ^{3}He (<10 ppm ^{4}He). In the liquid experiments, the fluorocarbon microspheres were

completely bathed in the liquid, and both were contained by the cells to be described below. For the monolayer work, the preparation recipe was based on the isothermal adsorption of ^{3}He at 4.2 K, Refs. 37 and 39. After the substrate surface had been cleaned, the ^{3}He was introduced to the experimental cell at 4.2 K until the pressure was approximately 0.3 bar. The cell was then pumped moderately for about 15 h. The impedance between the pump and the cell was essentially that of a capillary tube, 4 m long and 0.2 mm i.d., thermalized at 4.2 K. The residual pressure in the cell was then less than 1 Torr. From the work of Friedman *et al.*,[37,39] the quantity of adsorbed gas corresponding to an atomic monolayer could be determined to within a 5% uncertainty. All the experimental studies of the ^{3}He-^{19}F interaction have been conducted with microspheres which were annealed for 3 h at 295 °C, see Sec. II B 1. However, the presence of electronic impurities in the unannealed powder are interesting in certain respects. We have used the unannealed microspheres in a dynamic nuclear polarization experiment, Sec. V D. Before beginning any experiment, regardless of the use of annealed or unannealed microspheres, the cell was pumped during a 1-d period while being heated to 60 °C and subsequently flushed several times with ^{3}He before being cooled to 4.2 K (see Sec. II). In the following subsections we shall describe the pertinent cryogenic, cell, and NMR details.

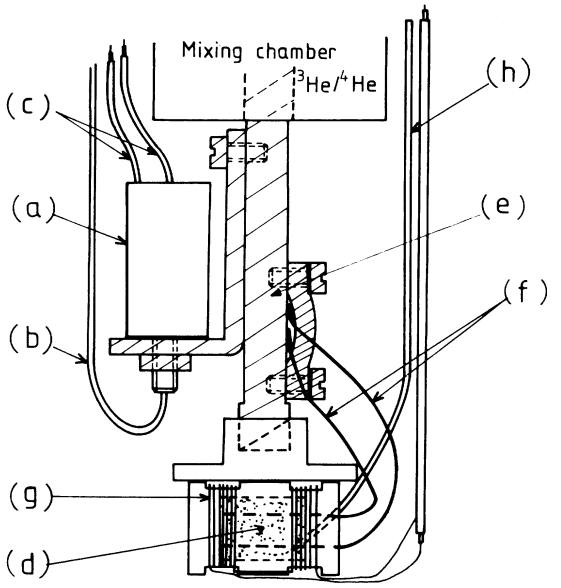

FIG. 8. Thermalization of the experimental cell. Melting-curve thermometer, (a), with filling line, (b), and coaxial cables for capacitance measurements, (c). The sample, (d), is in a plastic cell thermally connected to a silver rod, (e), through six silver wires, (f). NMR coil, (g), and filling capillary of the cell, (h), are also represented.

A. Cryostat and thermometry

Although the most efficient method for cooling a sample is to place it in the mixing chamber of the dilution refrigerator, we have placed our experimental cells outside the mixing chamber in order to avoid a parasitic NMR signal from the ^{3}He atoms in the refrigerator mixture, Fig. 8. The external thermalization was provided by an annealed silver rod, 6 mm in diameter. Four disks, 1 cm in diameter and 1 mm thick, of sintered silver powder (1 μm French powder) provided a large specific surface area, $S \sim 4 \times 10.2$ m^2, and were fixed to the end of the mixing chamber. Figure 8 shows the part of the rod which remains outside the mixing chamber. The experimental cells were thermalized by annealed silver wires with their number varying between one to seven, depending on the particular cell.

The temperature of the mixing chamber was determined from a calibrated 75-Ω Matsushita resistor. We have also used a ^{3}He melting-curve thermometer (MCT),[63] Fig. 9, attached to the silver rod, Fig. 8. For each experiment, the MCT capacitance was measured as a function of pressure at 4.2 K by means of a room-temperature manometer (Digi Quartz 2900 AS) with absolute precision of 5 mbar between 0 and 50 bars. The capacitance was measured with a bridge system based on an inductance divider (Dekatran DT 72 A). The reference capacitor consisted of a ceramic condenser, nominally 10 pF, situated in vacuum and thermalized to the 1.4 K ^{4}He cold plate of the cryostat. For temperatures greater than 30 mK, the temperature $T_{\rm MCT}$, read from the MCT,[64] was in excellent agreement with the temperature extracted from the ^{19}F magnetization, assuming it follows a Curie law.[23] A typical comparison between $T_{\rm MCT}$ and $M_{\rm F}^{-1}$ is presented in Fig. 10. When the temperature was less than 30 mK, the two thermometers indicated different values arising from different resistivities of the thermal paths. For example, the minimum temperature read from the MCT was approximately 8 mK, while the ^{19}F never indicated temperatures below 11 mK. For all $T < 30$ mK the temperature was measured from the ^{19}F system.

B. Experimental cells

During the course of this study we have used a variety of experimental cell designs. Each cell was constructed from Stycast 1266 epoxy, contained a chamber filled with DLX-6000 at a packing fraction of approximately 0.7, and possessed a (0.2×0.6)-mm^2 ^{3}He filling capillary. Additional important details particular to each cell are given below.

1. $\chi(P,T)$ and low-frequency $T_{1,2}$ cell

Figure 11 shows the cell which has been used to measure the magnetization of the liquid as a function of temperature and pressure, $M_{\rm He}(P,T)$. The thermalization of the sample region was made by six silver wires, 0.5 mm in diameter, which traversed the sample region. The external ends of the wires were in good thermal contact with the mixing chamber of the dilution refrigerator via an intermediate silver rod, Fig. 8. In order to conduct the experiments of $M_{\rm He}(P,T)$ at pressures above 29.3

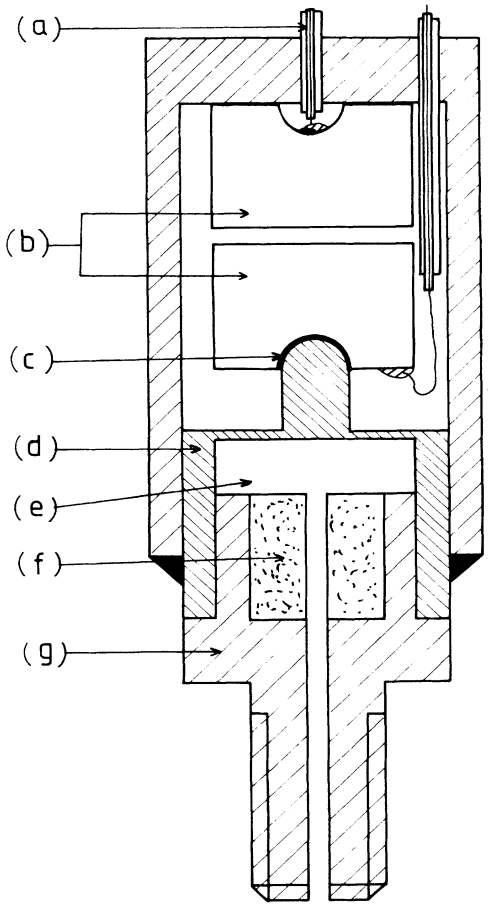

FIG. 9. Melting-curve thermometer: (a) coaxial cable, (b) electrodes of the capicitance, (c) Stycast isolator film, (d) Cu-Be diaphragm, (e) ^{3}He space, (f) sintered silver, and (g) silver body.

bars, we have incorporated a pressure gauge into the cell, Fig. 11. A low-temperature gauge is necessary because a solid ^{3}He plug forms in the capillary for $P > 29.3$ bars and excludes external measurement of P. The *in situ* manometer simply consists of a thin plastic membrane forming one wall of the cell, Fig. 11. In other words, the cell behaves in the same manner as the MCT,

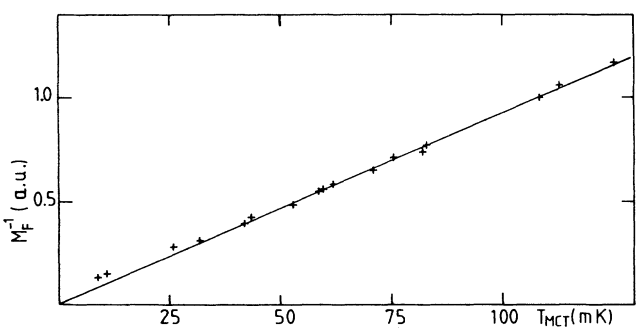

FIG. 10. Calibration of the fluorine magnetization against the temperature given by the melting-curve thermometer.

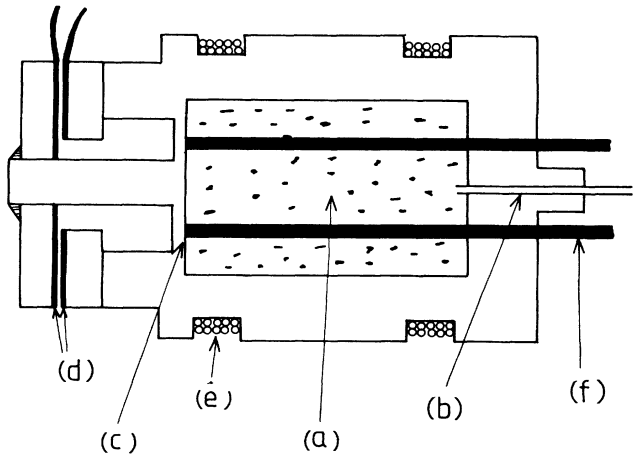

FIG. 11. Experimental cell used for the measurement of $\chi(P,T)$: (a) sample, (b) capillary for ^{3}He, (c) thin membrane, (d) capacity for the pressure measurement, (e) NMR coil, and (f) six silver wires for the thermalization.

and it was calibrated and operated in the same fashion; see preceding subsection. The precision of the cell pressure was on the order of 50 mbar. The demagnetization and low-field $T_{1,2}$ experiments were conducted in a similar cell which did not possess the pressure-gauge feature. For these cells, the NMR emitting and receiving coils were the same, Fig. 11.

2. *High-frequency T_1 cell*

Figure 12 shows the cell which was used for the high-frequency T_1 studies and the work of Schuhl *et al.*[16] The thermalization of the sample region was provided by a single silver wire, 1 mm in diameter. The NMR emission coil did not touch the cell, but was thermalized to the 1.4 K shield. The NMR receiving coil, Fig. 12, was oriented perpendicularly to the emitting coil and was glued to the cell wall.

3. *Dynamic nuclear polarization cell*

Figure 13 shows the details of the cell used in the dynamic nuclear polarization investigations and the heat-

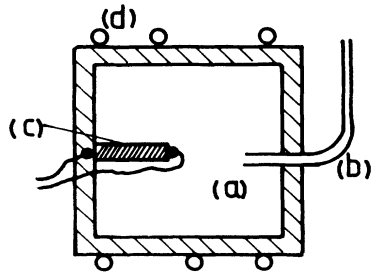

FIG. 12. Drawing of the cell used for high-frequency experiment: (a) fluorocarbon microspheres, (b) filling capillary, (c) a carbon-resistor thermometer, and (d) NMR coil. Thermalization was performed through the NMR coil.

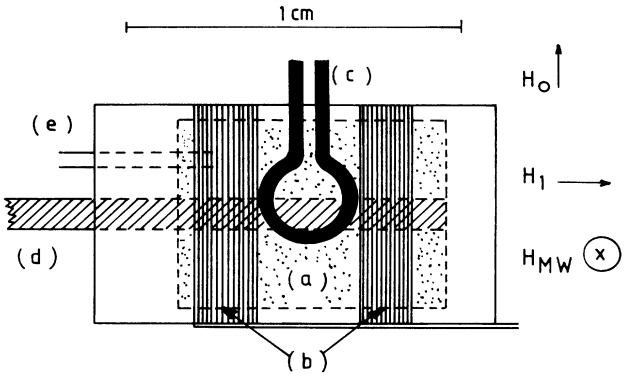

FIG. 13. Schematic drawing of the cells used for the dynamic nuclear polarization: (a) the location of the fluorocarbon beads, (b) a (2×80)-turn Helmholtz NMR coil providing the H_1 field, (c) the one-turn microwave coil providing the H_{MW} field, (d) a 1-mm-diam Ag wire providing thermal contact with a 6-mm-diam Ag rod connected to the mixing chamber, and (e) a filling capillary for ^{3}He. The cell is located in a high homogeneous superconducting solenoid providing the H_0 field.

ing experiments. Thermal contact between the cell and the silver rod of the mixing chamber, Fig. 8, was made via a 1-mm-diam silver wire which traversed the cell and contained no additional heat-exchanger elements. A single coil, glued to the cell wall, provided the emitting and receiving NMR fields and was perpendicularly oriented with respect to the irradiating rf coil, which was thermalized to the 1.4 K shield, Fig. 13. With the use of an experimental configuration which consisted of substituting the coils labeled (b) and (c) in Fig. 13 with a suitable EPR coil, the absorption line of the electronic impurities of the sample was studied.

C. NMR spectrometer

For the studies presented in this work, we have covered a large range of magnetic fields corresponding to ^{3}He frequencies between 125 kHz and 100 MHz. In every case the static magnetic or external demagnetizing field was applied by a superconducting solenoid situated in the liquid-^{4}He bath. Our measurements have been of three types: (i) magnetization measurements deduced from the surface of an adsorption signal at the frequency of the nuclear magnetic resonance; (ii) studies of the relaxation times of the longitudinal magnetization M_Z realized by observing the return to equilibrium of M_Z after a $\pi/2$ rf pulse which tips the magnetization into the plane perpendicular to the static magnetic field; and (iii) investigations of the relaxation time of the transverse magnetization by the method of spin echos. Several detection systems have been necessary to cover the large frequency range of our work. In all cases the variable capacitor of the resonant circuit was located outside the cryostat, i.e., approximately 150 cm from the inductance coil in which the sample was located. This long distance between the two components of the resonant circuit decreases the experimental resolution of the ^{3}He and ^{19}F signals. On the other hand, the arrangement offers a great amount of flexibility and permits a variation of resonant frequencies without thermally recycling the sample. For example, measurements performed at 25, 50, and 100 MHz were conducted with one low-temperature coil and did not require a warming of the sample above 1 K.

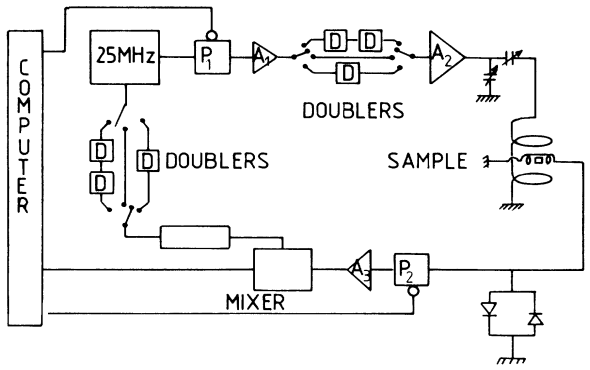

FIG. 14. High-frequency NMR spectrometer.

1. *High-frequency NMR spectrometer*

A schematic of our pulsed, high-frequency NMR electronics arrangement is shown in Fig. 14. The sample was surrounded by two perpendicularly crossed coils; one was used for the rf tipping pulse and the second for the signal detection. The receiving coil was glued to the experimental cell. The emitting coil, which was larger in diameter, was situated so as to avoid touching the cell and was thermalized to the 1.4 K shield.

The radiofrequency (rf) generator was a quartz synthesizer (Rhode and Schwarz, Model SMS) operating at 25 MHz. The rf pulse emitted from port P_1, Fig. 14, was amplified by a large-band commercial amplifier and subsequently reamplified by a high-powered narrow-band amplifier composed of a series of class-C transistors. In order to work at 50 and 100 MHz, the frequency was doubled, once or twice, before the final stages of high-powered amplification. We have obtained rf pulses with 300 Vpp at 50 MHz.

The receiving system was protected by D_L diodes and by the port P_2, which was closed during the emission of a rf pulse, Fig. 14. The signal was then amplified by a

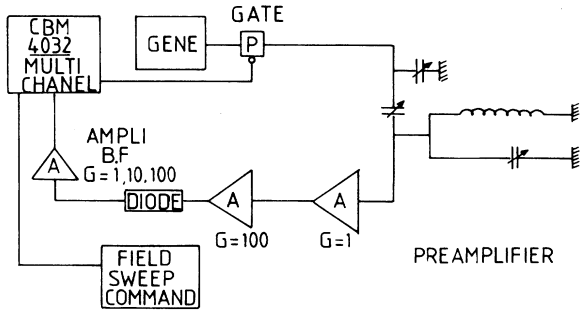

FIG. 15. Low-frequency NMR spectrometer.

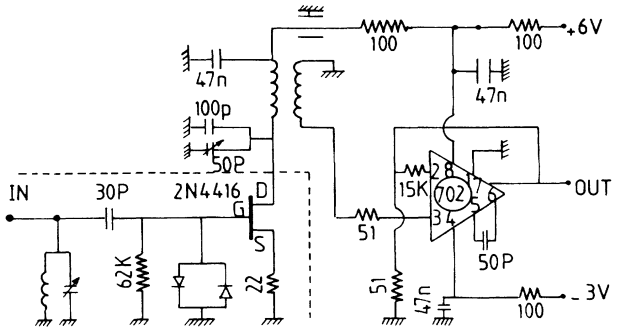

FIG. 16. Low-frequency preamplifier.

large-band, low-noise amplifier and passed into a mixer. The mixer reference came from the synthesizer and passed through a dephaser to permit the adaption of its phase to that of the received signal. At 50 and 100 MHz the reference signal passed through one or two doublers. Ports P_1 and P_2 were commanded by a minicomputer (Commodore 4032), which also recorded the signal. The minimum pulse duration was 10 μsec.

The continuous-wave NMR experiments were performed at fixed frequency by sweeping the magnetic field. The field sweep was commanded by the minicomputer, which had been transformed into a multichannel device. The received signal amplified once by a large-band amplifier, diode-detected, and subsequently recorded by the computer.

2. *Low-frequency NMR spectrometer*

For the studies at low frequencies, we have used a single, low-temperature coil for both emission and detection. Figure 15 shows a schematic of the electronics used for frequencies less than or equal to 1.45 MHz. In order to increase the sensitivity of the signal, we have used a low-noise, tuned preamplifier. The 1.45 MHz preamplifier is shown in Fig. 16.

The measurements of the susceptibility were performed over a period of more than six weeks In order to ensure the quantitative coherence of all the results, we have regularly calibrated the system by observing the response to a reduction of the rf level by 4%. Figure 17 shows typical ^{3}He and calibration signals. The detected fluctuations on the surface of the calibration signals were always less than 2%, and we have taken these shifts into account when determining M_{He}.

IV. STATIC MEASUREMENTS

A. Experimental results

We have measured the variation of the ^{3}He magnetization M_{He} confined by the fluorocarbon microspheres between 13 and 150 mK in a magnetic field $B=45$ mT and for pressures P between 0.4 and 32.0 bars. The results at $P=0.4$ bar are shown in Fig. 18. The variation of M_{He} with T can be separated into the sum of two contributions: the first, dominating above 30 mK, varies slightly with temperature, while the second, on the other hand, is important below 30 mK and depends strongly on T. The variation of $M_{\mathrm{He}}(T)$ presented in Fig. 18 may be perfectly reproduced by attributing the first contribution to N_L spins with a susceptibility χ_L given by bulk liquid ^{3}He at $P=0.4$ bar, and the second to N_S paramagnetic spins obeying a Curie law. The total susceptibility is then the sum of the two terms, i.e.,

$$\frac{M_{\mathrm{He}}(T)}{B}=N_L\chi_L(T)+N_S\chi_S(T)\ , \tag{14}$$

where B is the magnetic field. In this expression, we have implicity assumed that N_L and N_S are independent of (T). (The thermal expansion of liquid ^{3}He affects, for T up to 0.1 K, the $T=0$ value of N_L by less than 0.1%, and the possible solidification of the first liquid layer should not occur in the low temperature range $T<50$ mK where the sensitivity in determining N_L and N_S is maximum.) Using the experimental values of M_{He} and

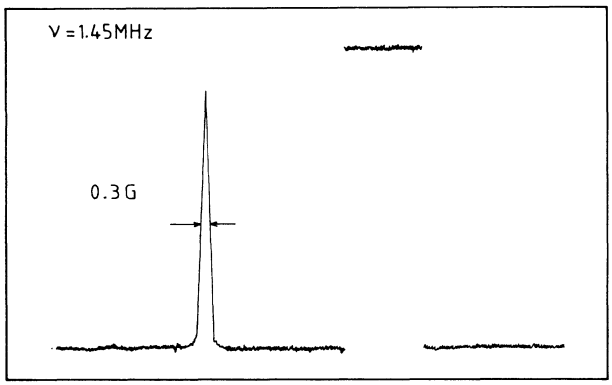

FIG. 17. cw-NMR ^{3}He signal (left) and calibration pulse (right).

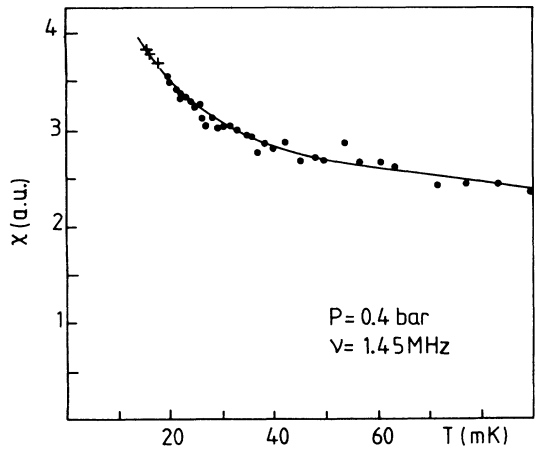

FIG. 18. Susceptibility of liquid ^{3}He confined by the DLX-6000 as a function of temperature.

the values of $\chi_L(T)$ at 0.4 bar deduced from the data of Ramm *et al.*,[12] we have plotted the variations of $M_{He}/\chi_L(T)$ in arbitrary units versus $\chi_S(T)/\chi_L(T)$ (Fig. 19), where a Curie law is assumed for $\chi_S(T)$. The points in Fig. 19 fall on a straight line, in perfect agreement with Eq. (14). In Fig. 19 the y-axis intercept and the slope of the line are proportional to N_L and N_S, respectively. However, our measurements do not enable us to determine the two parameters N_L and N_S, but only N_L/N_S.

In order to know the number of atomic layers involved in the Curie-type contribution, we have measured the ratio, N_F/N_{He}, between the number of ^{19}F spins, N_F, and the total number of ^{3}He spins, N_{He}. The determination method is identical to that used in Ref. 16 to measure the ratio between N_F and the number of ^{3}He spins contained in the first adsorbed layer, N_0. This procedure involves a comparison of the NMR signal surfaces of the two spin species at fixed frequency, i.e., slightly different fields, and at fixed temperature, typically 800 mK. The reduction of the ratio $\chi_L(T)/\chi_S(T)$ must be taken into account in this procedure. The ratio n defined by the number of Curie-type atoms, N_S, to N_0, is then given by

$$n=\frac{N_S}{N_S+N_L}\frac{N_{He}}{N_F}\frac{N_F}{N_0}\ . \tag{15}$$

The ratio N_F/N_0 was measured[16] in an experimental cell different from the one used here. However, measurements of gas adsorption at high temperatures[38] have shown that N_0 does not depend on the packing fraction of the DLX-6000 in the cell. It is therefore reasonable to use the previously measured[16] value of $N_F/N_0=207$ ($\pm 10\%$). The ratio N_L/N_S was not the same for the two cells we used since their packing fractions were slightly different, $N_L/N_S=32$ and 46. Combining the above numbers with the measured N_{He}/N_F values of each cell into Eq. (15) yields

$$n=1.4\pm 0.2\ . \tag{16}$$

This value is in good agreement with the value $n=1.5$ obtained by Hammel.[18] We note that the average density of the adsorbed ^{3}He atoms is certainly smaller than the density of the ^{3}He in the first adsorbed layer. In the case of Grafoil, the only substrate for which the adsorbed ^{3}He densities are known,[3,65] the ratio between the densities of the first and second layers is 1.3. By using this value for our substrate and supposing that the Curie-Weiss-type susceptibility only arises from the localized spins, i.e., solidlike spins, we can deduce that at $P=0.4$ bar the second layer is about 50% ($\sim 0.4\times 1.3$) solid.

The experimental values of M_{He} have been treated in the same manner for every pressure, and all the results can be expressed by a generalization of Eq. (14), i.e.,

$$\frac{M_{He}(P,T)}{B}=N_L(P)\chi_L(P,T)+N_S(P)\chi_S(T)\ . \tag{17}$$

The variation of $M_{He}/\chi_L(P,T)$ in arbitrary units with $\chi_S(T)/\chi_L(P,T)$ is presented in Fig. 20 for three pressures, 0.4, 11.0, and 32.0 bars. Similar results have been observed at 3.2, 16.0, 21.3, and 27.4 bars. For one pressure that was studied, $P=29.75$ bars, we have observed a different high-temperature behavior, Fig. 21. At temperatures higher than 100 mK, there is a disagreement between the experimental points and the straight-line fit to the low-temperature data. As we shall discuss below, the surface adsorption potential, V_B, introduces a lowering of the melting curve for the atoms near the surface. Thus, one expects, for temperatures above $T_c(V_B)$, to observe an increase in N_S, and consequently, an increase in the slope of the line, Fig. 21. However, the range of temperature, where Eq. (17) is valid, is sufficient for determining N_L/N_S at 29.75 bars and $T=0$. We have verified, using the values of V_m of Ref. 66, that the ratio

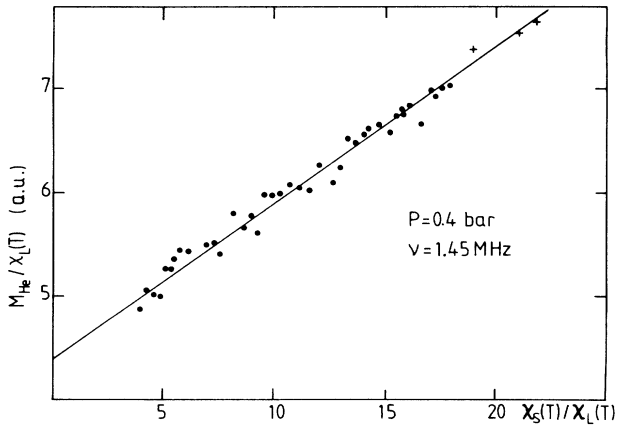

FIG. 19. Determination of the ratio between the Curie-Weiss contribution and the Pauli contribution to the susceptibility following Eq. (14). The slope of the straight line is proportional to N_S and the y-axis intercept to N_L.

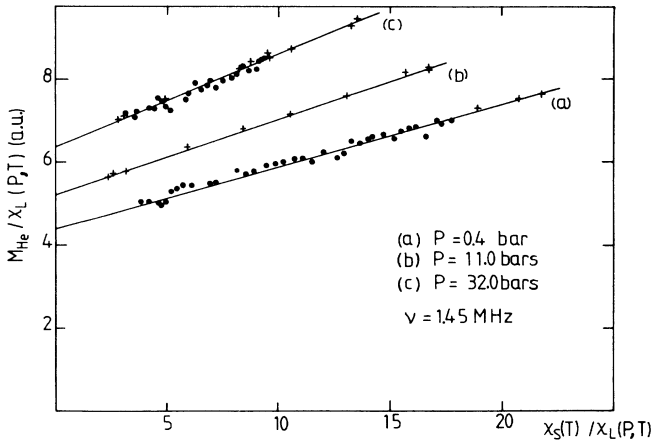

FIG. 20. Determination of N_L/N_S for three different pressures, Eq. (17).

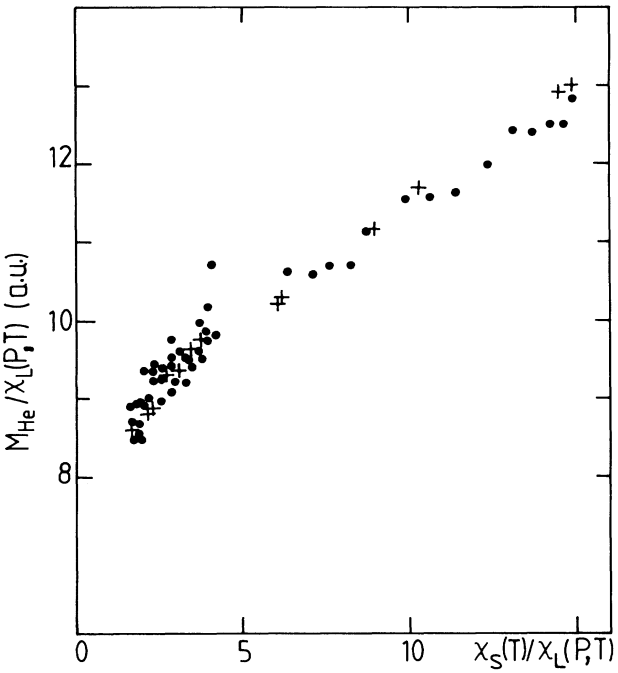

FIG. 21. At 29.7 bars, we have observed deviations to the linearity at high temperature.

$$\frac{N_L(P)V_m(P)}{N_L(0)V_m(0)}$$

was independent of pressure, Fig. 22. The small but notable increase of N_S with P (Fig. 22) reaches 60% of N_S (0.4 bar) at 32 bars. [The corrections due to the change of the free space in the cell with P can be estimated to be negligible. Firstly, one should consider the compression

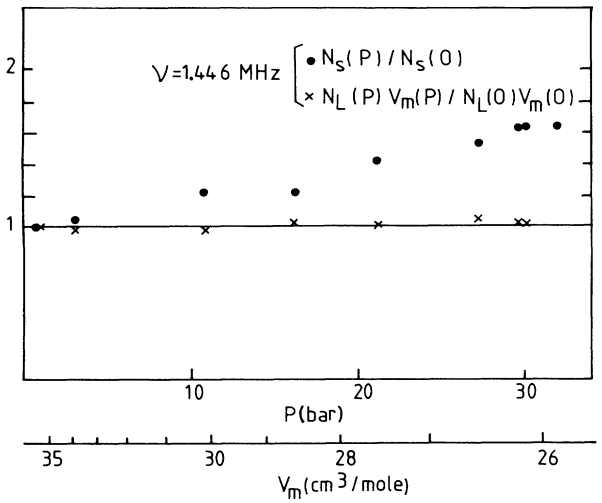

FIG. 22. Dependence of N_S with P. The data are normalized to the $P=0.46$ bar value. The crosses are the product of $N_L(P)$ and the molar volume of the liquid, $V_m(P)$, normalized by the $P=0.4$ bar values.

of the substrate. The volume variation may be estimated by using the Young's-modulus value determined at 4.2 K in Ref. 67, $E=217$ kg/mm^2, and this gives $\Delta V/V\sim 5\times 10^{-3}$. Secondly, we have estimated a change of the cell volume of $\Delta V/V\sim 3\times 10^{-3}$ in using $E=700$ kg/mm^2 for the Young's modulus of Stycast 1266 (Ref. 67). Finally, the surface solid ^{3}He volume increases with pressure and reduces the free space available for liquid by a quantity $\Delta V/V$ of the order of -1%.]

B. Continuous solidification model

The purpose of this subsection is to demonstrate that the pressure dependence of the Curie-Weiss contribution to the susceptibility of ^{3}He confined by fluorocarbon microspheres may be interpreted as a displacement of the solid-liquid interface in a surface potential V_B varying continuously with the distance to the substrate. We will consider here that the influence of the adsorption potential on the liquid may be represented by an increase of the liquid pressure. The liquid close to the interface will be taken to be equivalent in all its properties to a bulk liquid ^{3}He at a pressure higher than the applied pressure. In this approach our measurements indicate a growth of the solid atoms as the pressure is increased: $N_S(32 \text{ bars})=1.6N_S(0.4 \text{ bar})$.

The interface between solid and liquid is located at a distance from the surface that ensures that the pressure at the interface, P_i, is equal to the solidification pressure P_f. This pressure is (Fig. 23) the sum of the applied pressure P_a and the pressure induced by the van der Walls forces coming from the substrate. When P_a varies at constant temperature the interface should displace to ensure that $P_i=P_f$.[68] The number of adsorbed atoms then increases with P_a. A continuous growth of the solid may be observed with the substrate we have used because of its strong heterogeneity. With a perfect plane substrate, steps should be observed in $N_S(P)$. Let us present a thermodynamical analysis of this process in the $T=0$ limit. The chemical potentials of liquid and solid are identical at the interface. Since the liquid close to the interface is in equilibrium with the liquid located away from the interface, the chemical potential of the solid at the interface is equal to the chemical potential of the liquid located away from the interface:

$$U_s^i+V_B(Z_i)-U_l^a=-P_f v_s+P_a v_l \ , \tag{18}$$

where v_s and v_l are the molar volume of the solid and liquid, respectively, U_s^i the solid internal energy at the interface, and U_l^a the liquid internal energy away from the interface. A small variation of the applied pressure gives

$$dV_B=-v_s dP_f+v_l dP_a \ . \tag{19}$$

The same procedure applied for the equilibrium between the liquid at the interface and the liquid away from the interface leads to

$$dV_B=-v_l(P_f)dP_f+v_l(P_a)dP_a \ . \tag{20}$$

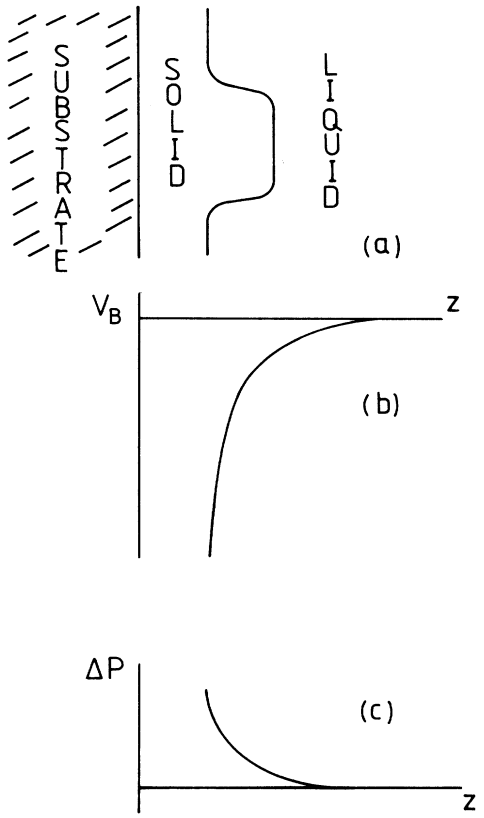

FIG. 23. Representation of (a) the adsorbed-solid–liquid interface, (b) the variations of the adsorption potential V_B, and (c) the induced overpressure ΔP as function of the distance to the substrate.

It follows from the preceding two equations that the interface pressure P_f is independent of the applied pressure P_a, and we assume that it is equal to the three-dimensional (3D) bulk melting pressure:

$$P_f = 34.34 \text{ bars} \quad \text{at } T = 0 \ .$$

We then have

$$V_B(P_a) = \int_{P_a}^{34.34} v_l dP_a \ . \tag{21}$$

This expression gives us an estimation of the dependence of V_B at the interface as the applied pressure increases from 0 to P_f (Table IV).

In order to compare this estimation with our experimental data, an expression of V_B as function of N_S should be written. This can be obtained using two approximations: firstly, we suppose that V_B varies like Z^{-3}, where Z is the distance to the substrate, and secondly, we consider that the solid is the addition of a dense adsorbed atomic layer with a molar volume v_s^0 plus a less dense solid of molar volume v_s. Let us call S the total surface; then,

$$N_S(P) - N_S(0.4) = \frac{S}{v_s}[Z(P) - Z(0.4)] \ ,$$

which may be written as

$$\frac{N_S(P)}{N_S(0.4)} - 1 = \frac{SZ(0.4)}{N_S(0.4)} \frac{1}{v_s} \left[\frac{Z(P)}{Z(0.4)} - 1 \right] .$$

Such an expression is reasonable for a substrate like our fluorocarbon microspheres, whose surface inhomogeneities completely smooth the steps in the isothermal adsorption of solid ^{3}He. On this substrate the adsorption potential V_B at the interface between the solid and the liquid ^{3}He may be considered to be a continuous function of N_S. With a homogeneous substrate, the following steps should be observed (Fig. 24).

We define ε by

$$1 - \varepsilon = \frac{SZ(0.4)}{N_S(0.4) v_s} = \frac{v_s^0 + (n-1)v_s}{n v_s} \ , \tag{22}$$

where n is the ratio between the number of atoms adsorbed at 0.04 bar and the number of atoms in the first atomic layer. We obtain for $V_B(P)$ the following expression:

$$\frac{V_B(P)}{V_B(0.4)} = \left| \frac{N_S(P)/N_S(0.4) - \varepsilon}{1 - \varepsilon} \right|^{-3} . \tag{23}$$

TABLE IV. Comparison of a thermodynamical determination of the adsorption potential V_B at the ^{3}He liquid-solid interface as a function of pressure (third column), with an estimation (fifth and sixth columns) deduced from the experimental values of $N_S(P)/N_S(0.4$ bar) (fourth column). The parameter ε is defined in Eq. (22).

P (bar)	V_B (K) [Eq. (21)]	$\frac{V_B(P)}{V_B(0.4)}$	$\frac{N_S(P)}{N_S(0.4)}$	$\frac{V_B(P)}{V_B(0.4)}$ [Eq. (23)] $=0.2$	$=0.3$
0.4	−11.8	1.00	1	1	1
3.2	−10.7	0.90	1.05	0.83	0.81
11.0	−7.7	0.65	1.22	0.48	0.44
16.3	−5.8	0.49	1.22	0.48	0.44
21.3	−4.1	0.35	1.42	0.28	0.24
27.4	−2.2	0.21	1.53	0.22	0.18
30.15	−1.3	0.11	1.63	0.17	0.15

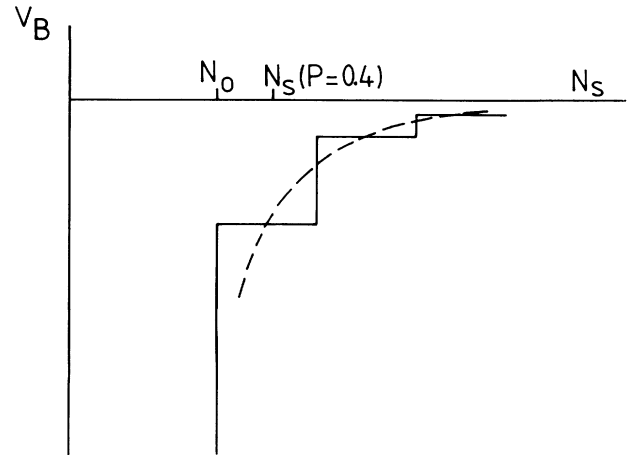

FIG. 24. Adsorption potential V_B for a ^{3}He atom located at the solid-liquid interface as function of the number of adsorbed ^{3}He atoms: for homogeneous (solid line) and inhomogeneous (dashed line) substrates.

In Table IV we present the value of the ratio $V_B(P)/V_B(0.4)$ deduced from the experimental determination of $N_S(P)/N_S(0.4)$ for different pressures. The agreement with values of the same ratio calculated from Eq. (21) is good if one takes into account the crudeness of the model. It is important to note that the peculiar behavior of the datum at 16.3 bars, Fig. 22 and Table IV, is not believed to be related to experimental error. In fact, the hint of a step in the variation of N_S with P, Fig. 22, might be interpreted as reminiscent of an adsorption step corresponding to the completion of the second layer: the experimental value $N_S=1.22N_S(0.4)$ at 11 and 16.3 bars is close to the value $1.26N_S(0.4)$ deduced from our crude model of adsorption.

In conclusion, the above thermodynamical description of the growth of adsorbed solid is in agreement with our experimental data, the quantity of adsorbed atoms being determined in this model by the solid-liquid thermodynamic equilibrium. We do believe that the entire Curie-Weiss contribution to the susceptibility of liquid ^{3}He confined by fluorocarbon microspheres is due to solid atoms adsorbed on the substrate. The possibility of a ferromagnetic liquid layer proposed several years ago[5,69] does not seem to be relevant for this substrate.

V. DYNAMIC MEASUREMENTS

A. $T_1 \propto T$ and the HR model

A universal, substrate-independent property of the spin-lattice relaxation time of ^{3}He, T_1^{He}, in a confined geometry is its linear temperature dependence. Hammel and Richardson[24] (HR) have proposed a model which explains this temperature dependence. The HR model is based on three assumptions, and several of these ideas have enjoyed a long history of discussion in the literature.[71]

(i) *The intrinsic relaxation of the liquid is negligible, and its magnetization relaxes only through the adsorbed surface layer.*

This is widely accepted as being true because the relaxation times of the confined liquid are factors of 10^2-10^3 shorter than the relaxation time of the bulk liquid.

(ii) *A rapid magnetization exchange is assumed to exist between the liquid and the adsorbed solid, ensuring that the system, even when out of external equilibrium, is in local equilibrium, i.e., the "magnetization potentials" are equal.*

For a bulk-liquid–bulk-solid interface, one may reasonably estimate the particle exchange frequency between the two phases $\nu_{L\text{-}S}$ to be a value between the bulk-solid exchange frequency ($\sim$10 MHz) and the bulk-liquid exchange frequency ($\sim$1 GHz). This estimate provides a magnetization transfer much faster than the relaxation processes ($\sim$1kHz).[17] However, in our experimental configuration the adsorption potential generated by the substrate could possibly reduce the mobility of ^{3}He atoms through the solid-liquid interface. Nevertheless, in order to show the existence of this rapid magnetization exchange even in our configuration, we have performed an experiment showing that it is possible to increase the magnetization of the liquid by heating the lattice baths of the ^{19}F and ^{3}He in a time short compared to the global relaxation of the system. The details of this experiment are provided in Sec. V C. It is therefore reasonable to conclude that $\nu_{L\text{-}S} \gg (T_{1S})^{-1}$ and that $\nu_{L\text{-}S} \gg (T_{2S})^{-1}$, since $T_{1S} > T_{2S} \sim 10^{-3}$ sec. Castaing and Nozières[70] have discussed a rapid exchange of spins at a liquid-solid interface by introducing an effective magnetic field, B_{eff}, which is different than the external static magnetic field, B_0. This approach permits us to write the ^{3}He magnetization as

$$\frac{M_S}{M_S^0}=\frac{B_{\text{eff}}}{B^0}=\frac{M_L}{M_L^0}\ , \tag{24}$$

where M_L^0 and M_S^0 are the respective equilibrium values of M_L and M_S, the instantaneous liquid and solid ^{3}He magnetizations. This formulation is completely equivalent to the HR approach,[24]

$$\frac{M_L-M_L^0}{M_L^0}=\frac{M_S-M_S^0}{M_S^0}\ . \tag{25}$$

(iii) *T_{1S}, the spin-lattice relaxation time of the adsorbed solidlike layer is assumed to be temperature independent.*

We recall that the relaxation of the solid layer is comprised of various processes: the relaxation through the ^{19}F due to the ^{19}F-^{3}He coupling, an intrinsic relaxation of the adsorbed layer in the absence of the liquid, and a relaxation introduced by atomic motion in the adsorbed layer due to the exchange between the solid and liquid. The fact that all of these mechanisms involve, under one form or another, the quantum exchange between the atoms of ^{3}He, lead HR to propose that T_{1S} is independent of temperature. We note that this assumption is not *a priori* evident. For bulk solid ^{3}He in high magnetic fields, the spin-lattice relaxation time varies strongly with temperature.[51,71] At sufficiently low tem-

perature, the exchange-lattice coupling is much weaker than the exchange-Zeeman coupling, which is indeed a temperature-independent mechanism. Experiments performed with a monolayer of ^{3}He adsorbed on Grafoil[65] have shown that the relaxation rate for the adsorbed film does not vary between 30 mK and 1 K. The same behavior has been observed for the fluorocarbon microspheres between 50 and 800 mK, Ref. 16. Consequently, assuming T_{1S} to be temperature independent seems justifiable.

In terms of the above three assumptions, the only source of the ^{3}He magnetization relaxation arises from the atoms in the surface layer, and we may write

$$\frac{dM_{\rm He}}{dt}=\frac{M_{\rm He}-M^0_{\rm He}}{T_1^{\rm He}}=\frac{M_S-M_S^0}{T_{1S}} . \tag{26}$$

The "magnetization potentials" are assumed to be equal during the relaxation, and this idea can be expressed as

$$M_{\rm He}=M_L+M_S=M_S\left[1+\frac{M_L}{M_S}\right]=M_S\left[1+\frac{M_L^0}{M_S^0}\right] . \tag{27}$$

Combining Eqs. (26) and (27) yields

$$T_1^{\rm He}=T_{1S}\left[1+\frac{M_L^0}{M_S^0}\right] . \tag{28}$$

For temperatures less than the magnetic Fermi temperature, T_F^{**} ($=360$ mK at $P=0$),[12,66] the equilibrium magnetization of the liquid and the solid may be written as

$$M_L^0=N_L\frac{C}{T_F^{**}},\quad M_S^0=N_S\frac{C}{T} . \tag{29}$$

Substitution of Eq. (29) into Eq. (28) yields

$$T_1^{\rm He}=T_{1S}\left[1+\frac{N_L}{N_S}\frac{T}{T_F^{**}}\right] . \tag{30}$$

Thus, the model predicts that $T_1^{\rm He}$ varies linearly with T between the limits

$$\frac{N_S T_F^{**}}{N_L}<T<T_F^{**} . \tag{31}$$

Equation (30) is in good agreement with our experimental results,[17] Fig. 25. In addition, the model predicts a plateau in the variation of $T_1^{\rm He}$ at the lowest temperatures when the solid magnetization becomes comparable to that of the liquid. This plateau has been effectively observed at Cornell with the fluorocarbon microspheres[18,23,24] and at Grenoble with alumina powder.[7] For $T>T_F^{**}$, Eq. (30) is no longer valid, and from Eq. (28) one expects to observe a weakening of the growth of the function $T_1^{\rm He}(T)$. Figure 26 shows our results at 50 MHz for temperatures between 30 and 800 mK and clearly shows the agreement between the HR model and the experimental results even at high temperatures, $T>T_F^{**}$.

The hypotheses upon which the HR model is based

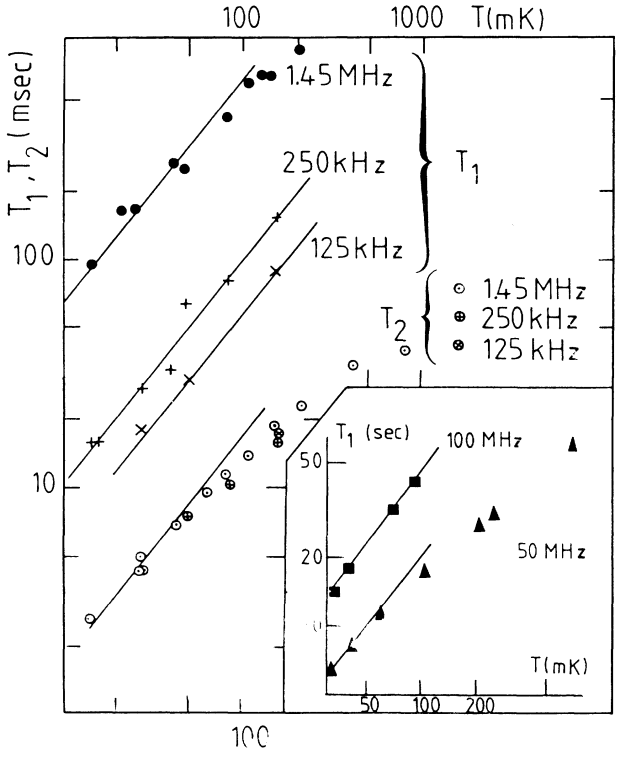

FIG. 25. T_1 and T_2 relaxation times of liquid ^{3}He confined by fluorocarbon microspheres are shown as a function of temperature. The frequencies correspond to the ^{3}He nuclear Larmor frequencies where the measurements were performed. The solid lines represent linear fits to the low temperature ($\lesssim 100$ mK) data. T_1: ●, 1.45 MHz; +, 250 kHz; ×, 125 kHz; T_2: ⊙, 1.46 MHz; ⊕, 250 kHz; ⊗, 125 kHz. Inset: ■, 100 MHz; ▲, 50 MHz.

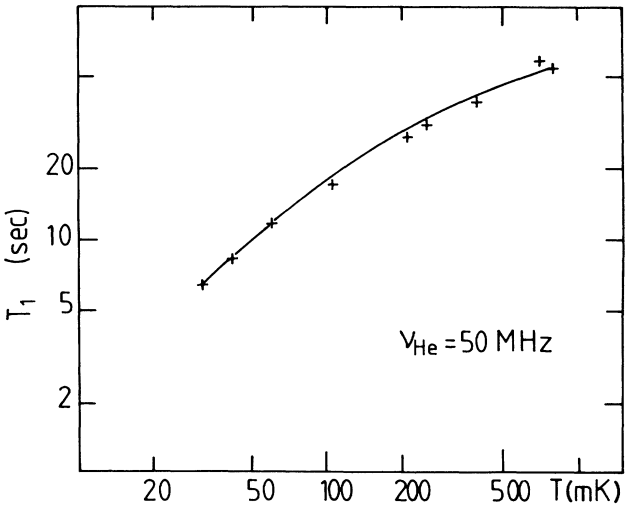

FIG. 26. Experimental relaxation times of liquid ^{3}He compared to the model of Hammel and Richardson. The solid line is from Eq. (28).

are also applicable to the transverse relaxation. After a $\pi/2$ pulse on the ^{3}He, all the spins precess at the Larmor frequency and remain in phase during a time of the order of the spin-spin relaxation time. Since the interface particle exchange is expected to be faster than T_{2S}, the "magnetization potentials" of the transverse magnetization of the two phases are identical during the transverse relaxation. Consequently, we obtain an expression similar to Eq. (30) for the transverse magnetization, namely

$$T_2^{\mathrm{He}} = T_{2S}\left[1+\frac{N_L}{N_S}\frac{T}{T_F^{**}}\right] . \tag{32}$$

This expression is in good agreement with our measurements of T_2^{He} shown in Fig. 25.

B. Demagnetization experiments

1. Monolayer

We have attempted to obtain information about the exchange in the ^{3}He monolayer by cooling it below 1 mK. It has been possible to obtain a ^{19}F spin temperature $T_{S,\mathrm{F}}=0.15$ mK by rapidly ($\sim$250 sec) lowering the magnetic field from an initial value of $B_i=3.1$ T to a final field of $B_f=18$ mT. The experimental cell we have used for this demagnetization experiment is presented in Fig. 13. In this experiment, we hoped the lattice of the ^{3}He would be cooled while the ^{19}F spin specific heat remained rather large. If this was possible, the Kapitza resistance controlling the thermal exchanges between the lattice and the exterior cell would increase considerably and provide complete isolation of the experimental cell. A new temperature would then be established in the cell in a time faster than the global thermal relaxation time of the cell. The measurement of M_{F} would provide a means of determining this new temperature $T=T_0M^0/M_{\mathrm{F}}$, which would enable us to follow $M_{\mathrm{He}}(T)$. The evolution of M_{He} and M_{F} after lowering the field is shown in Fig. 27. The magnetizations have been normalized to their final equilibrium values, M_{F}^f and M_{He}^f, taken at the end of the relaxation at $T_0=21$ mK. Immediately after the stabilization of the magnetic field at a value B_f, the magnetizations have the following values:

$$M_{\mathrm{F}}/M_{\mathrm{F}}^f=140, \quad T_{S,\mathrm{F}}=0.15 \text{ mK} ,$$

$$M_{\mathrm{He}}/M_{\mathrm{He}}^f=94, \quad T_{S,\mathrm{He}}=0.22 \text{ mK} .$$

The magnetizations were observed to relax in parallel with a characteristic time on the order of 9 min. The relaxation rate increased near the end of the run and reached, at 21 mK, the value of $T_1^{\mathrm{F}}=60$ sec, which is identical to what has been measured by the saturation technique. This decrease in the relaxation time at ultralow temperatures is compatible with a decoupling between the Zeeman baths and the mixing chamber of the cryostat. However, it is difficult to know if the decoupling is associated with lattice-exterior interaction (path 4 of Fig. 6) which is weak or, on the other hand, with the lattice-exchange mechanism (path 3 of Fig. 6). In this latter case, given our present understanding of the magnetization exchange between the two Zeeman baths, Sec. II C 2, the M_{F} measures the ^{19}F magnetization but not the corresponding ^{3}He spin temperature. This possibility might explain why the ratio $M_{\mathrm{F}}/M_{\mathrm{He}}$ remained constant during the entire relaxation and why no indication of ordering in M_{He} was observed. In conclusion, the monolayer demagnetization experiments as performed here did not permit a determination of the presence or absence of a strong exchange constant in the adsorbed layer. A colder lattice would be needed to control the thermodynamics of the system.

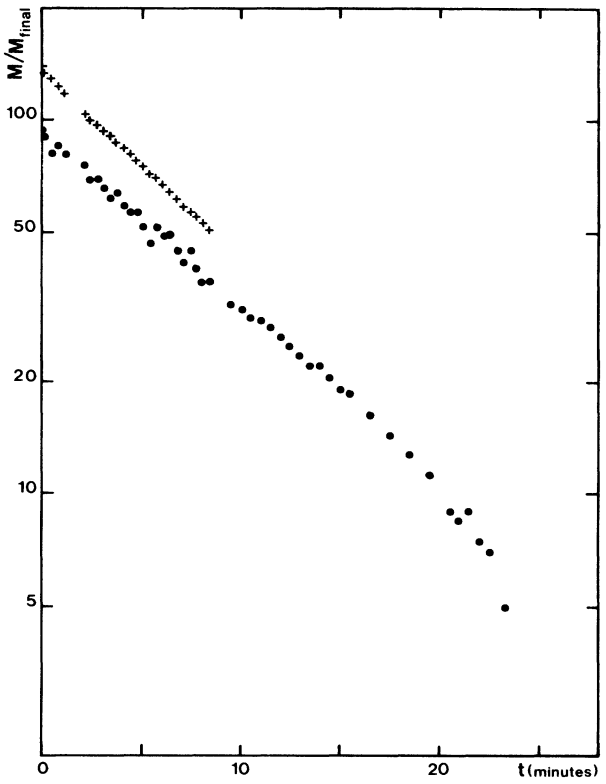

FIG. 27. Relaxation of the magnetizations of the ^{19}F and of one adsorbed layer of ^{3}He just after the field has been decreased from 3 to 0.015 T. The final temperature is 21 mK.

2. Liquid

For these investigations, the experimental method and the cell were the same as those for the monolayer studies. The essential differences were that the cell was full of liquid and that the temperature was on the order of 100 mK. Figure 28 shows the M_{F} and M_{He} evolution after lowering the magnetic field from 10 to 1.1 kG. The two curves were obtained for two identical demagnetizations at a temperature of 100 mK. The shift between the two traces is not significant because the initial times were different. The ^{3}He magnetization, which is essentially that of the liquid, relaxes exponentially with a characteristic time T_{des} equal to the ^{19}F relaxation time, which is much longer than the ^{3}He relaxation time. At

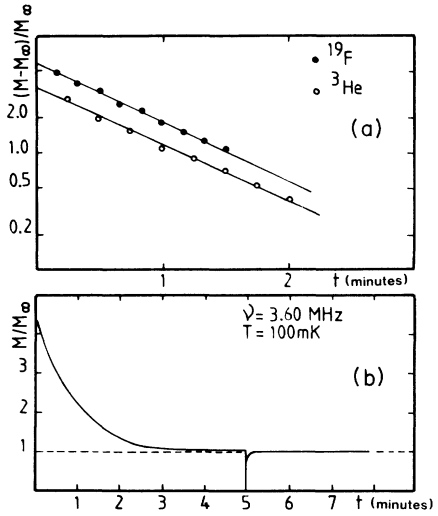

FIG. 28. (a) Relaxation of the magnetizations of the ^{19}F and liquid ^{3}He after the field has been decreased. (b) The relaxation of the liquid is compared to the relaxation after a $\pi/2$ pulse on the ^{3}He at $t=5$ min.

100 mK and in 1.1 kG, $T_1^F=55$ sec and $T_1^{He}=0.5$ sec. During the demagnetization, the liquid magnetization appears to be retained by an interaction with the solid ^{3}He. This process would consist of an exchange of magnetization between the two components and is not unexpected. We have summarized the characteristics of some demagnetizations in Table V. A quantitative interpretation seems rather arduous, because our experimental method was intrinsically nonstationary. A proper analysis would require the incorporation of the relative magnitudes of all the relaxation rates between various energy baths of the system and the simultaneous measurement of M_F and M_{He}. However, these liquid demagnetizations do provide qualitative information on the character of the exchange between the liquid and the solid. In particular, our results are clearly incompatible with a temperature exchange model.

C. Heating experiments

In this subsection we will describe an experiment which clearly shows that the magnetization transfer between solid and liquid ^{3}He remains faster than any relaxation, even when the solid is localized by the adsorption potential of a substrate. This experiment was performed in a magnetic field $B_0=450$ G corresponding to a ^{3}He Larmor frequency $\nu_{He}=1.45$ MHz. The cell (Fig. 13) was maintained initially at $T_i=15$ mK. Next, the lattice temperature of the sample was suddenly increased by an uncalibrated heat pulse on the silver rod which thermally connected the sample cell to the mixing chamber of the dilution refrigerator. The time constant of the lattice temperature response may be considered to be shorter than the ^{19}F relaxation time ($T_{1,F}=15$ sec at 1 MHz). The evolutions of ^{19}F and ^{3}He magnetization, M_F and M_{He}, are presented in Fig. 29. Immediately after the heat pulse, M_{He} increases to about twice its initial value. Then both magnetizations relax together with a time constant $\tau=T_{1,F}=15$ sec. The final equilibrium value of M_F is smaller than the initial one, M_F^i, by a factor 2.6. This corresponds to an equilibrium temperature $T^f=38$ mK. The final value of M_{He} is slightly smaller than its initial value, as is expected for $T^f=38$ mK, since M_{He} is essentially due to the temperature-independent liquid magnetization.

The increase of M_{He} is a direct consequence of the fast magnetization transfer between the two ^{3}He phases [Eq. (24)]. This point can be illustrated briefly. The ^{19}F-^{3}He coupling is due to a fast magnetization exchange between the two spin species.[16] This leads to a relation identical to Eq. (24), namely

$$\frac{M_F}{M_{F,0}}=\frac{M_S}{M_{S,0}} \ . \tag{33}$$

Using Eq. (24), we then obtain

$$\frac{M_F}{M_{F,0}}=\frac{M_S}{M_{S,0}}=\frac{M_L}{M_{L,0}} \ . \tag{34}$$

Just after the heat pulse, the lattice temperature was about 38 mK. The fluorine magnetization, which is unchanged by the heat pulse, is then larger—by a factor 2.6—than the new equilibrium value. The liquid equilibrium magnetization is temperature independent. To follow Eq. (34), M_L must increase. This rise is possible since $M_F \gg M_{He}$, and any change in M_{He} does not notably affect M_F+M_{He}.

D. Dynamic nuclear polarization of liquid ^{3}He

The presence of a large concentration of electronic impurities (2×10^{18} cm^{-1}) in uncleaned fluorocarbon microspheres (DLX-6000) offers the possibility of enhanc-

TABLE V. Parameters of some demagnetization with liquid ^{3}He in the cell.

Field (initial) (T)	Field (final) (T)	Temperature (mK)	M_{He}/M_{He}^0	T_{des} (sec)	T_1^F (sec)	T_1^{He} (sec)
3	0.11	100	10.4	58	55	0.45
1	0.11	100	4.6	53	55	0.45
3	0.03	30	20	14	15	0.12
1	0.03	30	8	16	15	0.12

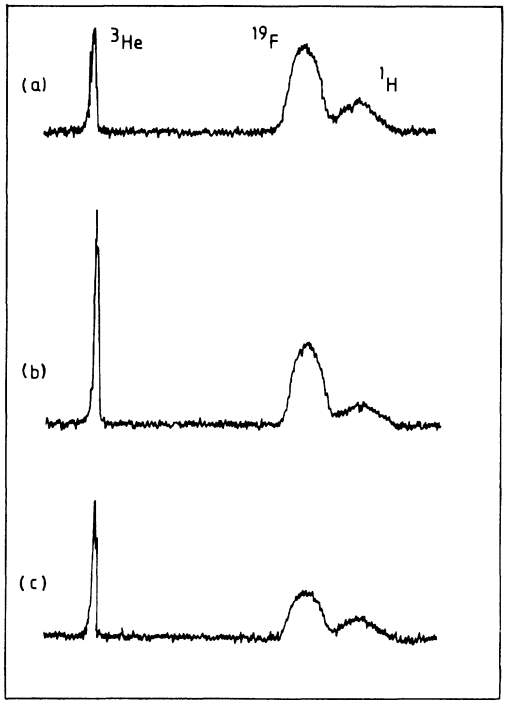

FIG. 29. cw-NMR signal of ^{3}He, ^{19}F, and ^{1}H spins: (a) at the equilibrium at $T_i = 15$ mK; (b) immediately after a heat pulse on the lattice baths; (c) 15 sec later. The NMR frequency is 970 kHz and the final temperature is 38 mK.

ing the nuclear fluorine magnetization, M_F, by dynamic nuclear polarization (DNP). This polarization method is based[72] on the existence of a dipolar interaction between electronic and nuclear spins. In the simplest picture, DNP may be viewed as a microwave cooling of the electronic spin-spin reservoir which subsequently reduces the spin temperature of surrounding nuclei.[72] This may be accomplished by external microwave irradiation at a frequency which differs slightly from the electronic Larmor frequency ν_e, i.e., $\nu = \nu_e + \Delta$. This irradiation may produce an increase ($\Delta < 0$) or a decrease ($\Delta > 0$) of the nuclear polarization relative to its equilibrium value. The rapid magnetization transfer occurring at both substrate-adsorbed ^{3}He and solid-liquid ^{3}He interfaces transmits the polarization enhancement of M_F to the liquid ^{3}He.

We have performed experiments in small magnetic fields ($B \lesssim 300$ G) and have demonstrated the validity of the above-proposed method.[73] We have been able to use this method to produce liquid ^{3}He with a polarization larger than its $T = 0$ equilibrium value, in a temperature range (50–250 mK) where the Fermi-liquid ^{3}He is degenerate. Typical results of DNP on liquid ^{3}He at 300 G are presented in Fig. 30. An appropriate choice of the irradiation frequency gives positive or negative polarization enhancements of liquid ^{3}He.

Recent experiments[74] have shown the possibility of applying the DNP process presented here to different substrates. We believe that an appropriate choice of the substrate, a better microwave device, and a perfect knowledge of the spin dynamics of a mixed (i.e., ^{3}He-^{4}He) adsorbed film should permit polarizations larger than 10% to be achieved.[73]

E. $T_{1,Z}(\nu)$

We have seen that the measurement of the relaxation time of confined ^{3}He, T_1^{He}, gives access to the relaxation time of the adsorbed layer. In particular, in the range of temperature where T_1^{He} varies linearly with T, the coefficient [Eq. (30)] is proportional to

$$T_{1S}\frac{N_L}{N_S}\frac{1}{T_F^{**}} .$$

Our experiments have been performed with two distinct cells, one for the low frequencies ($\nu \leq 1.45$ MHz) and another for high frequencies ($\nu \geq 25$ MHz). In order to deduce the frequency dependence of T_{1S} from these measurements, we have measured the ratio N_L/N_S for both of our experimental cells from the variation of M_{He}

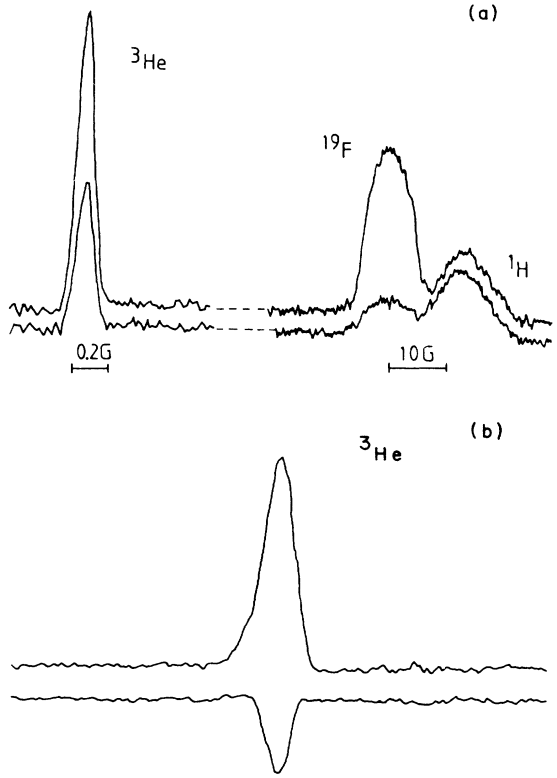

FIG. 30. Typical results of (a) positive and (b) negative DNP are shown when 0.6 layers of ^{4}He are present on the fluorocarbon-^{3}He interface. The NMR frequency is 970 kHz. In (a) the cw-NMR signals of the three nuclear species ^{3}He, ^{19}F, and ^{1}H, left to right, are shown, at $T = 250$ mK before microwave irradiation (lower curve) and after 6 min of irradiation at $\Delta = -20$ MHz (upper curve). The enhancement factors are $\alpha_F = 4.6$ and $\alpha_{He} = 2.0$. In (b) only the ^{3}He signal is shown at $T = 150$ mK, before (upper curve) and after irradiation at $\Delta = 20$ MHz (lower curve).

with the temperature at $P=0.4$ bar (see Fig. 19). The difference between the results of the two cells is less than the experimental errors. We are therefore able to consider our two cells as strictly identical with $N_L/N_S=46\pm2$, at $P=0$.

In Fig. 31 we have plotted the frequency variation of the relaxation of ^{3}He. The points in the figure correspond to the coefficients of proportionality between T_1^{He} and T, in the temperature range where the dependence is linear (Fig. 25). In Fig. 31 the crosses represent the values obtained at Cornell[18,23,24] at 2 and 4 MHz, normalized by a factor 46/200, because in their experiments the ratio N_L/N_S was 200. Together, these measurements reveal a linear variation of the relaxation time, T_{1S}, with frequency, where

$$\frac{T_1^{He}}{T\nu_{He}}=4.1 \text{ sec/K MHz} \tag{35}$$

and

$$\frac{T_{1S}}{\nu_{He}}=32 \text{ msec/MHz} .$$

The frequency-independent value for T_2, i.e., the slope of T_2^{He}/T (represented by a dashed line in Fig. 31), yields

$$T_{2S}=1.3 \text{ msec} .$$

In a certain way, we have obtained information on the properties of the solid adsorbed layer which are more detailed than those results from experiments with an isolated monolayer. There are three reasons for this apparent paradox.

(i) *The reproducibility of the sample.* We have noted several quantitative variations between two distinct "monolayers," i.e., on their relaxation-time values. This effect arises because the study of the monolayer over a large range of frequency requires a change of the NMR coil. Therefore, the necessary warming destroys the initial sample conditions.

(ii) *The size of the signal.* The liquid provides us with an amplifier for both the signal and relaxation time. The measurements of T_1 at low frequency are limited on the monolayer by the weak-signal value.

(iii) *The thermalization.* The lattice of the two-dimensional film has a small specific heat. The true thermal reservoir is then situated outside the cell. It is necessary to take into account a possible decoupling between the lattice and the external thermal reservoir which complicates the analysis.

However, the presence of the liquid perturbs the properties of the adsorbed layer. The number of adsorbed atoms is larger than one monolayer; thus there are localized solid atoms in weak potential wells. In the second layer, V_B is about an order of magnitude weaker than for the first layer. The additional solid atoms are less dense. The movements of exchange are then more rapid. Finally, the solid atoms are able to exchange with the atoms of the liquid. The mobility of the localized atoms may be therefore strongly increased by the presence of the liquid.

The relaxation mechanism in solid ^{3}He is a modulation of ^{3}He-^{3}He dipolar interactions induced by the movements of atoms. In the temperature range of our experiments the only relevant movements are due to vacancies or quantum exchange. The vacancies are very mobile in ^{3}He solid and may be considered delocalized under the form of vacancy waves.[32,50] Their concentration is determined by an activation energy and therefore varies rapidly with temperature. Hence the temperature-independent relaxation processes (T_{1S}) cannot be imputed to vacancies. It is therefore only the movement induced by the exchange that participates in the relaxation. We have dedicated the following section to the study of exchange in the solid film. We will present first the existing theoretical models in order to understand our experimental results [$T_{1S}(\nu)$, $T_{2S}(\nu)$] and then relate these results to the Curie-Weiss-type deviations observed in the temperature variation of the magnetization.

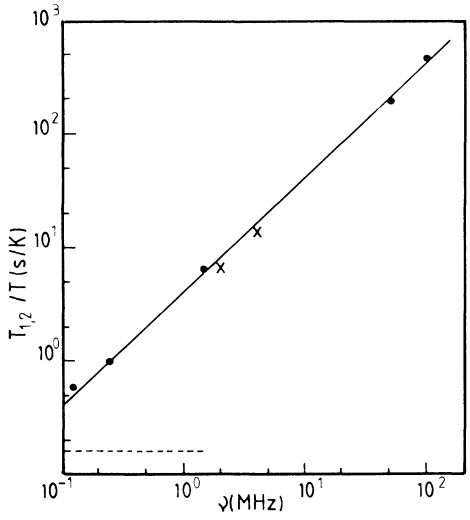

FIG. 31. The variation of the ^{3}He relaxation times are plotted as a function of the ^{3}He resonance frequency. The ● represent the slope, T_1/T, of the linear temperature dependence of T_1 as indicated by the solid lines in Fig. 25. The renormalized (see text) Cornell T_1/T data (Ref. 23) are denoted by ×. The solid line reflects the linear frequency dependence of the T_1/T data. The dotted line represents the frequency independence of T_2/T shown in Fig. 25.

VI. EXCHANGE IN THE ADSORBED SOLIDLIKE FILM

A. Theoretical models

1. Internal exchange

In the three-dimensional ^{3}He solid, the nuclear spins order antiferromagnetically at low temperature.[10] For the largest molar volume, $V_m=24.2$ cm^3/mol, the transition temperature is approximately 1.1 mK. This mag-

netic ordering is due to special properties of a quantum crystal of fermions and not, as usual, to dipolar magnetic interactions. In effect, the energies involved in the latter interactions are 3 orders of magnitude smaller than the observed transition temperature. The large zero-point energy leads to a strong quantum exchange. For two spin-$\frac{1}{2}$ particles, the degeneracy of the ground state is raised to a singlet state and a triplet state. The global wave function must be antisymmetric and the spin states therefore correspond to antisymmetric (singlet) and symmetric (triplet) functions. The energy separation of these two levels is related to the interaction between the two atoms, $V(r,r')$, which is relatively well approximated by the Lennard-Jones potential:

$$V(r,r')=4\varepsilon\left[\left[\frac{\sigma}{r-r'}\right]^{12}-\left[\frac{\sigma}{r-r'}\right]^{6}\right],$$

$$\varepsilon=-10.22\ \text{K}\ , \qquad (36)$$

$$\sigma=2.556\ \text{Å}\ .$$

The exchange interaction is then equivalent to an effective Hamiltonian acting on spins,

$$H=-2J\boldsymbol{\sigma}_1\cdot\boldsymbol{\sigma}_2\ , \qquad (37)$$

with

$$J=\int\int V(r,r')\phi_1(r)\phi_1^*(r')\phi_2^*(r)\phi_2(r')dr\,dr'\ ,$$

where ϕ_1 and ϕ_2 are the orbital wave functions on the two atom sites. In a solid the Hamiltonian can be generalized as

$$H=-2\sum_{i<j}J_{ij}\boldsymbol{\sigma}_i\cdot\boldsymbol{\sigma}_j\ . \qquad (38)$$

Several detailed theoretical studies (see, in particular, Ref. 75) have shown that circular exchange involving more than two atoms is favorable in solid ^{3}He than two-spin exchange. Roger[35] has applied the multiple-particle–exchange theory to the two-dimensional case. He has obtained a ferromagnetic ground state in agreement with experimental observations. His calculation of the variation of the exchange energy J as a function of the interatomic spacing is in good agreement with the experimental values deduced from relaxation time measurements of a ^{3}He monolayer adsorbed on Grafoil[76] (Fig. 32). The density of the first adsorbed layer varies slightly from one substrate to another since the adsorption potential may be quite different between two distinct substrates. Nevertheless, one may reasonably estimate, as a first approximation, the density of the first adsorbed layer to be the value obtained on Grafoil by neutron scattering.[3] This estimate gives an interatomic spacing close to 3.3 Å for this layer. The corresponding Curie-Weiss temperature is then rather small (Fig. 32), and would not explain the value $\Theta\sim0.5$ mK measured on different substrates.[6,9,18] Nevertheless, several arguments permit us to attribute the large value of Θ in this type of experiment to internal exchange of the solid film:

(i) We have shown that, in our case, the second atomic layer is partially solid and its density is smaller than the first layer.

(ii) Our substrate possess an inhomogeneous surface. Due to local topology, part of the atoms may be situated in cavities having a small accessible surface and others a large accessible surface. One might expect that the latter atoms have an exchange frequency much larger than the average value of the layer.

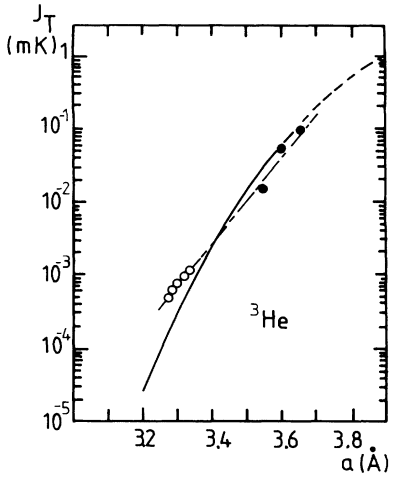

FIG. 32. Exchange constant for a triangular 2D lattice. The experimental data (○,●) are extracted from measurements on Grafoil (Ref. 76), and the theoretical line is from the multiple-exchange model (Ref. 35).

2. *Indirect exchange*

The presence of the liquid introduces particular exchange mechanisms into the adsorbed film. In 1977 Sokoloff and Widom[77] suggested an indirect RKKY-like exchange between the localized solidlike atoms mediated by the Fermi-liquid ^{3}He. These authors predicted a ferromagnetic interaction which was in agreement with experimental observations. This mechanism has subsequently been studied theoretically in detail by Jichu and Kuroda.[30] As is usual for the typical RKKY interaction,[78] the effective exchange frequency has been calculated by a second-order perturbation calculation. In performing their calculation, Jichu and Kuroda took into account two important modifications to the original RKKY model:

(i) The wave functions of the localized atoms have an extension of the order of k_F^{-1}, where k_F is the Fermi wave vector of liquid ^{3}He. The solid spins cannot therefore be considered pointlike.

(ii) The surface notably pertubes the wave functions of the quasiparticles in the direction normal to the surface, Z.

The exchange constant J_{ij} between two localized atoms, i and j, is then given by[30]

$$J_{ij}=4\left[\frac{k_F}{\pi\alpha}\right]^4\frac{V_0^2}{E_F R_{ij}^6}\exp\left[-\frac{2k_F^2}{\beta}\right]F(k_F R_{ij})\ , \qquad (39)$$

where

$$F(z)=\int_0^{\pi/2} d\theta \cos 2\theta \int_0^Z dx\, xJ_2(x)\sin(x\cos\theta)\ .$$

In this expression R_{ij} is the distance between the two spins i and j, E_F is the Fermi energy of the liquid ^{3}He, V_0 is the hard-core interaction between two ^{3}He atoms, β is the spatial extension of localized atoms in the surface plane, and $\alpha=(2mV_B)^{1/2}$, where m is the mass of localized atoms and V_B is their adsorption potential to the substrate. The function $J_2(x)$ is the second-order Bessel function. The value of J_{ij} decreases rapidly with the interatomic distance such that only the nearest-neighbor interaction is important.[30] In order to obtain a quantitative estimate, the authors have used the following parameters: $k_F=0.9$ Å^{-1}; $V_B=60$ K, which gives $\alpha=3$ Å^{-1}; the distance between two nearest neighbors $R=3.3$ Å; the interaction force is the same as for a liquid at zero pressure, $\rho(E_F)V_0=0.9$, where $\rho(E_F)$ is the density of states at the Fermi surface; and $\beta=1.5$ Å^{-2}. These values produce a value $J_{ij}=0.15$ mK for the exchange constant between two neighbors. The transition temperature is then $T_c=3\times 0.15=0.45$ mK for a triangular lattice.

It is interesting to note that the sign of the function $F(Z)$ changes for the value $Z=k_FR_{ij}=3.3$, whereas the parameters used by Jichu and Kuroda lead to $Z=2.97$. Such a model would predict an antiferromagnetic interaction either at high pressure since k_F(34 bars)/$k_F(0)=1.13$, or with a low-density solid since $a=3.7$ Å gives $k_FR_{ij}=3.33$ at $P=0$.

The other processes of indirect exchange that have been studied[29,30] have all provided a negative sign for the exchange constant J_{ij}, i.e., an antiferromagnetic ground state. Furthermore, the estimates of the absolute value of J permit one to neglect these possibilities in view of the RKKY exchange model described above.

B. Spectral density: Variation of T_1 with frequency

Our dynamic measurements presented in preceding section (Fig. 25) have shown a linear dependence of the relaxation time of the adsorbed film as a function of frequency up to at least 100 MHz (Fig. 31). Recent experiments made in Copenhagen indicate that this proportionality holds up to 180 MHz.[79] Since the relaxation process is a modulation of the dipolar interaction, T_1 is directly related to the spectral density, $J(\omega)$, of these modulations. Here we will neglect the double-frequency term (i.e., the flip-flip processes) in the expression of T_1, which is therefore proportional to $J^{-1}(\omega)$. The modulation movements are induced by the quantum exchange. Above a characteristic frequency which is of the same order as the exchange frequency, the spectra density goes to zero and the relaxation time T_1 [i.e., $J^{-1}(\omega)$] diverges more rapidly than any power of ω. It follows from our results that exchange frequencies, as large as 100 MHz$\sim$5 mK, exist in the ^{3}He adsorbed film. Moreover, the susceptibility measurements made at Cornell[18] indicate a Curie-Weiss temperature Θ close to 0.5 mK which corresponds to an average exchange frequency of the order of 3 MHz. These experimental results cannot be understood simultaneously in terms of a single exchange frequency, and a distribution in the exchange frequency is required. (Although generated by a different physical point of view, similar results and conclusions were generated by Monod and Cowen[25] on a Zeolite substrate and by Sullivan[71] who used Vycor.) The majority of ^{3}He atoms would have an exchange frequency less than or equal to that measured by the static susceptibility, while a small quantity of atoms would be responsible for the high-frequency relaxation. The physical reason for the existence of these large frequencies of exchange would be related to the inhomogeneities of the substrate. In fact, it is reasonable to imagine that a certain number of atoms are localized in surface cavities with an accessible volume which is, in some cases, much larger than the average molar volume of the layer. In the case of internal exchange, it is easy to show[15] that a linear variation of $J^{-1}(\omega)$, and therefore of $T_1(\omega)$, corresponds to a homogeneous distribution of the specific surfaces S_m.[80] From the experimental results of Ref. 76 presented in Fig. 32, we estimate the variation of the exchange frequency with the specific surface as

$$\omega_e=CS_m^{23}\ , \tag{40}$$

where C is a constant.

A homogeneous distribution $A(S_m)=$const (Fig. 33)[80] leads to a distribution of the exchange frequency given by

$$B(\omega_e)=C'\omega_e^{-0.96}\sim C'\omega_e^{-1}\ , \tag{41}$$

where C' is another constant.

To obtain the spectral density, one must consider the appropriate spectral density corresponding to each value of ω_e, $J_{\omega_e}(\omega)$. To simplify the discussion, we have approximated $J_{\omega_e}(\omega)$ by a step function of ω as shown in Fig. 34. This simplification does not affect the frequency dependence of $J(\omega)$ that will be obtained. The spectral density $J(\omega)$ is then given by

$$J(\omega)\sim\int_0^{\omega_c} J_{\omega_e}(\omega)B(\omega)d\omega_e\ ; \tag{42}$$

then, with Eq. (41) we obtain

$$J(\omega)\sim\left[\frac{1}{\omega}-\frac{1}{\omega_c}\right]C''\ ,$$

where C'' is a constant, and ω_c is the highest exchange

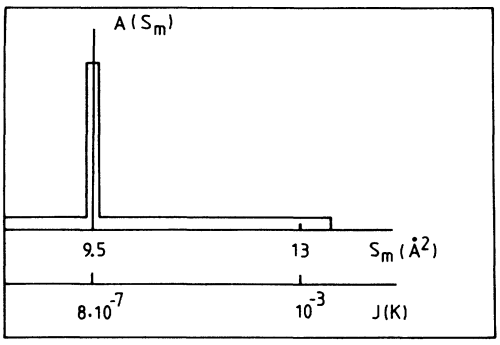

FIG. 33. Distribution of specific surface S_m, which would explain the linear spectral density (Fig. 31) (Ref. 80).

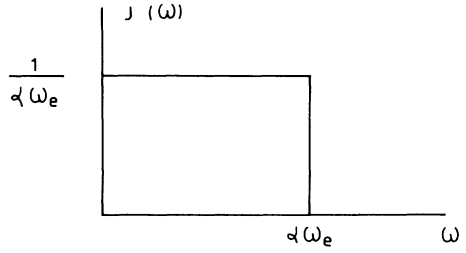

FIG. 34. Schematic spectral density considered for a simple exchange frequency system.

frequency, corresponding to the largest specific surface (Fig. 33).

In the framework of the analysis, the magnetization must follow a Curie-Weiss law, with a high-temperature value of Θ equal to the average value of all the spins i of Θ_i in each site. One also expects to observe deviations from the Curie-Weiss law when $T \sim \Theta$ since the spins corresponding to the highest exchange frequencies should be blocked. A rapid order-of-magnitude calculation indicates that in order to maintain a compatibility between our explanation for the variation of T_1 with ν, and with the observation of a Curie-Weiss temperature of 0.5 mK, one should consider that 20% of the atoms are associated with cavities that contribute to the higher specific surface homogeneous distribution. The remaining atoms should be localized with a small S_m corresponding to an interatomic distance of about 3.3 Å. This density is compatible with the experimental value measured on Grafoil[3] and corresponds to an exchange constant of a few microkelvin. A second independent estimate is in agreement with this value: interpolation of the variations of $T_{1S}(\omega)$ and $T_{2S}(\omega)$ (Fig. 31) indicates that the two curves would intercept at a frequency close to 40 kHz, which corresponds to 2 μK.

For $\omega_c \sim 200$ MHz, the number of atoms with $\omega_e > 10$ MHz would be equal to about 6% of the solidlike atoms. The precision of the experimental measurements of Hammel *et al.*[18] do not permit us to comment on the existence of the deviations predicted at $T \sim \Theta$ due to freezing of the high-frequency exchange spins.

The present analysis cannot be applied to the indirect-exchange process (Sec. VI A 2), since the exchange constant J_{ij}, calculated by Jichu and Kuroda,[30] depends only weakly on the density of adsorbed solid [Eq. (39)]. In effect, the linear dependence we have obtained for $T_1(\omega)$ is the combination of two factors: one part being a density distribution of S_m and the other an exchange constant varying rapidly with S_m. These considerations seem to indicate that the exchange observed by the susceptibility measurements would be a direct process. However, it is not, in our opinion, possible to conclude with the elements that we actually possess at this time. It is, in fact, troubling to observe comparable Curie-Weiss temperatures on homogeneous substrates like Grafoil[38] and on various inhomogeneous substrates.[18,9,6] We have not, up to now, incorporated into our discussion the characteristics of the relaxation processes on our substrate; the relaxation of the solid adsorbed film is due to both Zeeman-Lattice and ^{3}He-^{19}F couplings. Nevertheless, we have attributed these two channels to quantum exchange. As we take this complication into account, it does not contradict the qualitative analysis developed above. In addition, the persistence of the ^{3}He-^{19}F coupling with one adsorbed monolayer up to magnetic fields of the order of 3 T shows that there is, even in the absence of the liquid, some high-frequency exchange movements.

Additional experiments remain necessary in order to determine the nature of the exchange movements. For example, measurements of $T_1(\omega)$ on very homogeneous substrates like Grafoil up to at least 100 MHz would permit an investigation of the role played by the inhomogeneities in the linear dependence we have observed with our substrate (Fig. 31). Furthermore, the variation of Θ with pressure obtained from the susceptibility measurements at low temperatures (< 1 mK) would permit a choice between the two processes that have been discussed, provided the measurements are reproducible with fluorocarbon microspheres and with Grafoil. In particular, with a homogeneous substrate like Grafoil it is likely that the variation with pressure of the number of adsorbed atoms would exhibit steps corresponding to the solidification of successive layers. If the Weiss temperature Θ was due to an internal exchange, then at the solidification pressure, Θ must grow strongly when a new layer is solidified and subsequently decrease slowly with increasing applied pressure. The beautiful experiments of Franco *et al.*,[81,82] performed on films of ^{3}He with thicknesses between 1 and 7 atomic layers, lead one to believe that such a phenomena would be observable.

VII. SUMMARY

The study of the magnetic interaction between ^{19}F spins in fluorocarbon microspheres and ^{3}He spins adsorbed at the surface has shown the existence of rapid movements in the layer of adsorbed solid atoms, even down to temperatures of a few millikelvin. The magnetization transfer between the two nuclear species is mediated by a modulation of the ^{19}F-^{3}He dipolar interaction through the internal movements of the adsorbed ^{3}He layer. Only the movements introduced by the quantum exchange between ^{3}He nuclei explain simultaneously the efficiency of the coupling down to temperatures as low as 1 mK, and the constant relaxation rate of this coupling over close to 2 orders of magnitude in temperature.

The hypothesis that the exchange is responsible for the coupling is in good quantitative agreement with our measurements of the relaxation times measured at 25, 50, and 100 MHz with a monolayer adsorbed on the substrate. This leads to exchange frequencies up to at least 20 MHz when the density of this layer corresponds to a value 200 times smaller.

Our magnetization measurements of the liquid confined by fluorocarbon microspheres has enabled us to deduce the thickness of the ^{3}He solid film which separates the liquid and the substrate. For our sub-

strate, the number of solidlike ^{3}He atoms, N_s, varies smoothly with pressure from $1.4N_0$ at $P=0.4$ bar to $2.25N_0$ at $P=32$ bars (N_0 is the number of atoms contained in the first adsorbed layer). We have proposed a thermodynamic explanation of this weak variation, which is linked to the surface heterogeneity of the substrate that we have used. On such a surface, the adsorption potential V_B is a continuous function of N_s. When the liquid pressure increases, the ^{3}He-liquid–^{3}He-solid interface moves towards weaker potential V_B regions.

We have clearly demonstrated experimentally that the magnetization exchange between the adsorbed ^{3}He solid and the liquid is faster than all the relaxation processes. We have also *a posteriori* justified one of the hypotheses upon which the model of Hammel and Richardson is based. All of the liquid magnetization relaxes through the adsorbed layer where the processes of relaxation are independent of temperature. We have verified the validity of this model ($T_1/T=$const) over a larger range of magnetic fields (0.003–3.0 T). We have also generalized this model to the relaxation of transverse magnetization of the liquid ($T_2/T=$const). The slope of the line $T_1(T)$ provides access to the processes of magnetic relaxation of the adsorbed layer. Our study has shown that the relaxation time of the longitudinal magnetization of this layer, T_{1S}, is proportional to the magnetic field B between 0.003 and 3.0 T.

From all these results we are able to propose a description of the adsorbed ^{3}He layer that separates the liquid from the substrate. The inhomogeneous character of the substrate surface provides a distribution in the molar volume of the adsorbed layer. This gives rise to a corresponding distribution of the characteristic exchange frequency which, even in the first atomic layer, may cover several tens of MHz. This would explain the following.

(1) The ^{3}He-^{19}F coupling at high magnetic field, in spite of the large average density of the first adsorbed layer.

(2) The Curie-Weiss constant value of $\Theta=0.5$ mK.

(3) The proportionality between T_{1S} and T.

In addition, this description is consistent with a variation of N_S with P.

With the goal of testing this description, it seems to us important to perform the following experimental studies.

(1) Measurements of the susceptibility $\chi(P,T)$ down to temperatures below 0.5 mK, giving access to the variation of Θ with P.

(2) A study of the variation of T_{1S} with pressure should permit the extraction of the contribution of the relaxation due to the additional solidlike atoms.

(3) By reproducing these experiments on a homogeneous substrate, it would be possible to verify the role played by the surface heterogeneities of the substrate.

ACKNOWLEDGMENT

We would like to thank P. C. Hammel, R. C. Richardson, F. B. Rasmussen, N. S. Sullivan, M. Roger, and M. T. Béal-Monod for helpful discussions and interesting comments. We are grateful to M. Raynaud for sample preparation. One of us (M.W.M.) acknowledges the receipt of support by the North Atlantic Treaty Organization (NATO) via the U.S. National Science Foundation (NSF). Laboratoire de Physique des Solides is associated with the Centre National de la Recherche Scientifique (CNRS), France.

*Present and permanent address: Department of Physics, College of Liberal Arts, Kyoto University, Kyoto 606, Japan.

†Present address: Department of Physics, University of Florida, Gainesville, FL 32611.

[1]A review has been given by R. C. Richardson, Physica **126B**, 298 (1985).

[2]S. W. Sciver and O. E. Vilches, Phys. Rev. B **18**, 285 (1978).

[3]C. Tiby, H. Wiechert, H. J. Lauter, and H. Godfrin, Physica **107B**, 209 (1981).

[4]A. I. Ahonen, T. Kodama, M. Krusius, M. A. Paalanen, R. C. Richardson, W. Schoepe, and Y. Takano, J. Phys. C **9**, 1665 (1976).

[5]D. Spanjaard, D. L. Mills, and M. T. Béal-Monod, J. Low Temp. Phys. **9**, 307 (1979).

[6]A. I. Ahonen, T. A. Alvesalo, T. Haavasoja, and M. C. Veuro, Phys. Rev. Lett. **41**, 494 (1978).

[7]H. Godfrin, G. Frossati, D. Thoulouze, M. Chapellier, and W. G. Clark, J. Phys. (Paris) Colloq. **39**, C6-287 (1978).

[8]H. M. Bozler, T. Bartolac, K. Luey, and A. L. Thomson, Phys. Rev. Lett. **41**, 490 (1978).

[9]Y. Okuda, A. J. Ikushima, and H. Kojima, Phys. Rev. Lett. **54**, 130 (1985).

[10]D. D. Osheroff, M. C. Cross, and D. S. Fisher, Phys. Rev. Lett. **44**, 792 (1980); T. Hata, S. Yamasaki, M. Taneda, T. Kodama, and T. Shigi, Phys. Rev. Lett. **51**, 1573 (1983); E. D. Adams, Can. J. Phys. (to be published).

[11]Y. Takano, N. Nishida, Y. Miura, H. Fukuyama, H. Ishimoto, S. Ogawa, T. Hata, and T. Shigi, Phys. Rev. Lett. **55**, 1490 (1985).

[12]H. Ramm, P. Pedroni, J. R. Thompson, and H. H. Meyer, J. Low Temp. Phys. **2**, 539 (1970).

[13]See, for example, Y. Okuda and A. J. Ikushima, Phys. Rev. B **33**, 3560 (1986).

[14]A. Schuhl and M. Chappellier, in *Proceedings of the 17th International Conference on Low-Temperature Physics–LT-17,* Karlsruhe, 1984, edited by U. Eckern, A. Schmid, W. Weber, and H. Wühl (North-Holland, Amsterdam, 1984), p. 727.

[15]A. Schuhl, thèse d'Etat, Université Paris–Sud, 1986 (unpublished).

[16]A. Schuhl, F. B. Rasmussen, and M. Chapellier, J. Low Temp. Phys. **57**, 483 (1984).

[17]S. Maegawa, A. Schuhl, M. W. Meisel, and M. Chapellier, Europhys. Lett. **1**, 83 (1986).

[18]P. C. Hammel, Ph.D. thesis, Cornell University, 1983 (unpublished).

[19]D. F. Brewer, J. Low Temp. Phys. **3**, 205 (1970).

[20]M. T. Béal-Monod, Phys. Rev. B **28**, 368 (1983).

[21]J. Kelly and R. C. Richardson, in *Proceedings of the 13th International Conference on Low-Temperature Physics–LT-13, Boulder, Colorado, 1972,* edited by K. D. Timmerhaus, W. J. O'Sullivan, and E. F. Hammel (Plenum, New York, 1974), Vol. 1, p. 167.
[22]D. Wollhardt and P. Wölfle, Phys. Rev. Lett. **41**, 190 (1981).
[23]P. C. Hammel, M. L. Roukes, Y. Hu, T. J. Gramila, T. Mamiya, and R. C. Richardson, Phys. Rev. Lett. **51**, 2124 (1983).
[24]P. C. Hammel and R. C. Richardson, Phys. Rev. Lett. **52**, 1441 (1984).
[25]P. Monod and J. A. Cowen, Technical Report of the CEA, Saclay, 1967 (unpublished).
[26]A. L. Thompson, D. F. Brewer, and Y. Goto, in *Proceedings of the 14th International Conference on Low-Temperature Physics–LT-14, Otaniemi, 1975,* edited by M. Krusisus and M. Vuorio (North-Holland, Amsterdam, 1975), Vol. 1, p. 463.
[27]B. P. Cowan, J. Low Temp. Phys. **50**, 135 (1983).
[28]H. M. Bolzer, D. M. Bates, and A. L. Thomson, Phys. Rev. B **27**, 6992 (1983).
[29]M. Heritier, J. Phys. (Paris) Lett. **40**, L451 (1979).
[30]H. Jichu and Y. Kuroda, Prog. Theor. Phys. **67**, 715 (1982); **69**, 1358 (1983).
[31]M. T. Béal-Monod and S. Doniach, J. Low Temp. Phys. **28**, 175 (1977).
[32]R. A. Guyer, in *Proceedings of the Hakone International Symposium, 1977* (Physical Society of Japan, Tokyo, 1978), p. 178.
[33]M. Heritier and P. Lederer, Phys. Rev. Lett. **42**, 1068 (1979).
[34]S. V. Iordanskii, J. Low Temp. Phys. **40**, 401 (1980).
[35]M. Roger, Phys. Rev. B **30**, 6432 (1984).
[36]E.I. Dupont DeNemours and Co., Wilmington, DE 19898.
[37]L. J. Friedman, T. J. Gramila, and R. C. Richardson, J. Low Temp. Phys. **55**, 83 (1984).
[38]Y. J. Brown, J. Low Temp. Phys. **60**, 183 (1985).
[39]L. J. Friedman, P. J. Millet, and R. C. Richardson, Phys. Rev. Lett. **47**, 1078 (1981).
[40]J. P. Harrison, J. Low Temp. Phys. **37**, 467 (1979); A. R. Rutherford, J. P. Harrison, and M. J. Stott, J. Low Temp. Phys. **55**, 157 (1984).
[41]C. A. M. Castelijns, K. F. Coates, A. M. Guenault, S. G. Mussett, and G. R. Pickett, Phys. Rev. Lett. **55**, 2021 (1985); J. M. Parpia, Phys. Rev. B **32**, 7564 (1985).
[42]M. Chapellier, L. Sniadower, G. Dreyfus, H. Alloul, and J. Cowen, J. Phys. (Paris) **45**, 1033 (1984).
[43]W. B. Ard, H. Shields, and W. Gordy, J. Chem. Phys. **23**, 1727 (1955).
[44]E. E. Schneider, J. Chem. Phys. **23**, 978 (1955).
[45]D. Suryanarayana, L. Kevan, and S. Schlick, J. Am. Chem. Soc. **104**, 668 (1982).
[46]G. Dreyfus, J. Leviner, and M. Legrand, Phys. Rev. B **20**, 1720 (1979).
[47]M. Chapellier, J. Phys. (Paris) Lett. **40**, L143 (1979).
[48]S. F. Cox, V. Bouffard, and M. Goldman, J. Phys. C **6**, L100 (1973).
[49]M. Goldman, S. F. Cox, and V. Bouffard, J. Phys. C **7**, 2940 (1974).
[50]R. A. Guyer, R. C. Richardson, and L. I. Zane, Rev. Mod. Phys. **43**, 532 (1971).
[51]M. Chapellier, M. Bassou, M. Devoret, J. M. Delrieu, and N. S. Sullivan, J. Low Temp. Phys. **59**, 45 (1985).
[52]A. Landesman, Ann. Phys. (Paris) **8**, 53 (1970).
[53]R. Kubo and K. Tomita, J. Phys. Soc. Jpn. **9**, 888 (1954).
[54]R. Kubo, J. Phys. Soc. Jpn. **17**, 100 (1962).
[55]See, in particular, A. Avogradro and M. Villa, J. Chem. Phys. **66**, 2359 (1977).
[56]B. P. Cowan, J. Phys. C **13**, 4575 (1980).
[57]The considerations of a finite 2D system are discussed by J. P. Korb, M. Winterhalter, and H. M. McConnell, J. Chem. Phys. **80**, 1059 (1984).
[58]A. Abragam, *The Principles of Nuclear Magnetism* (Oxford University Press, New York, 1961), Chap. 8.
[59]See the detailed study of P. L. Kuhns, P. C. Hammel, and J. S. Waugh, Bull. Am. Phys. Soc. **31**, 242 (1986); P. C. Hammel, P. L. Kuhns, O. Gonen, and J. S. Waugh, Phys. Rev. B (to be published).
[60]M. Richards, in *Phase Transitions in Surface Films,* Vol. 51 of *NATO Advanced Study Institute, Series* B, edited by J. G. Dash and J. Ruvald (Plenum, New York, 1980).
[61]Q. Geng, M. Olsen, and F. B. Rasmussen, Jpn. J. Appl. Phys. **26**, Suppl. **26-3**, 329 (1987).
[62]M. W. Meisel, S. Maegawa, A. Schuhl, and M. Chapellier (unpublished).
[63]D. S. Greywall and P. A. Bush, J. Low Temp. Phys. **46**, 451 (1982).
[64]D. S. Greywall, Phys. Rev. B **17**, 2747 (1983).
[65]H. Franco, thèse d'Etat, CRTBT, Grenoble, 1985 (unpublished).
[66]J. C. Wheatley, Rev. Mod. Phys. **47**, 415 (1975).
[67]M. Van de Voorde, Cryogenics **8**, 296 (1976).
[68]The interfacial tension can be neglected, S. Balibard (private communication) and E. Rolley, S. Balibar, and F. Gallet, Jpn. J. Appl. Phys. **26**, Suppl **26-3**, 391 (1987). Consequently, the solid is formed on the surface of microspheres and not away from the walls, as it in more confined geometries. See, for example, M. Shimoda, T. Mizusaki, T. Suzuki, A. Hirai, and K. Eguchi, Phys. Lett. **102A**, 426 (1984); E. D. Adams, Y. H. Tang, K. Uhlig, and G. E. Haas, J. Low Temp. Phys. **66**, 85 (1987).
[69]M. T. Béal-Monod, Phys. Rev. B **28**, 368 (1983).
[70]B. Castaing and P. Nozières, J. Phys. (Paris) **40**, 257 (1979).
[71]N. S. Sullivan, J. Low Temp. Phys. **22**, 313 (1976).
[72]See the review given by A. Abragam and M. Goldman, Rep. Prog. Phys. **41**, 395 (1978).
[73]A. Schuhl, S. Maegawa, M. W. Meisel, and M. Chapellier, Phys. Rev. Lett. **54**, 1952 (1985).
[74]L. W. Engel and K. Deconde, Phys. Rev. B **33**, 2035 (1986).
[75]M. Roger, J. H. Hetherington, and J. M. Delrieu, Rev. Mod. Phys. **55**, 1 (1983).
[76]M. G. Richards, J. Phys. (Paris) Colloq. **39**, C6-1342 (1978).
[77]J. B. Sokoloff and A. Widom, in *Proceedings of the International Conference on Quantum Crystals,* Fort Collins, Colorado, 1977, edited by J. R. Sites (Colorado State University, Fort Collins, 1977).
[78]M. A. Ruderman and C. Kittel, Phys. Rev. **96**, 99 (1954); K. Yosida, *ibid.* **106**, 393 (1957).
[79]See Ref. 61.
[80]By specific surface, S_m, we mean the ratio between the surface area available for ^{3}He adsorption, due to pits and valleys in the microspheres, and the surface area of microspheres with a perfect spherical shape. The distribution function $A(S_m)$ is a spectrum of the aforementioned S_m values.
[81]H. Franco, H. Godfrin, and D. Thoulouze, Phys. Rev. B **31**, 1699 (1985).
[82]H. Franco, R. E. Rapp, and H. Godfrin, Phys. Rev. Lett. **57**, 1161 (1986).